Diameter and rigidity of multiwalled carbon nanotubes are critical factors in mesothelial injury and carcinogenesis

Hirotaka Nagai[a,b], Yasumasa Okazaki[a], Shan Hwu Chew[a], Nobuaki Misawa[a], Yoriko Yamashita[a], Shinya Akatsuka[a], Toshikazu Ishihara[a], Kyoko Yamashita[a], Yutaka Yoshikawa[c], Hiroyuki Yasui[c], Li Jiang[a], Hiroki Ohara[a], Takashi Takahashi[d], Gaku Ichihara[e], Kostas Kostarelos[f], Yasumitsu Miyata[g], Hisanori Shinohara[g], and Shinya Toyokuni[a,1]

[a]Department of Pathology and Biological Responses, Nagoya University Graduate School of Medicine, Nagoya 466-8550, Japan; [b]Department of Pathology and Biology of Diseases, Kyoto University Graduate School of Medicine, Kyoto 606-8315, Japan; [c]Division of Analytical and Physical Chemistry, Department of Analytical and Bioinorganic Chemistry, Kyoto Pharmaceutical University, Kyoto 607-8414, Japan; Departments of [d]Molecular Carcinogenesis and [e]Occupational and Environmental Health, Nagoya University Graduate School of Medicine, Nagoya 466-8550, Japan; [f]Nanomedicine Laboratory, Centre for Drug Delivery Research, School of Pharmacy, University of London, London WC1N 1AX, United Kingdom; and [g]Department of Chemistry and Institute for Advanced Research, Nagoya University, Nagoya 464-8602, Japan

Edited by David A. Tirrell, California Institute of Technology, Pasadena, CA, and approved October 19, 2011 (received for review June 22, 2011)

Multiwalled carbon nanotubes (MWCNTs) have the potential for widespread applications in engineering and materials science. However, because of their needle-like shape and high durability, concerns have been raised that MWCNTs may induce asbestos-like pathogenicity. Although recent studies have demonstrated that MWCNTs induce various types of reactivities, the physicochemical features of MWCNTs that determine their cytotoxicity and carcinogenicity in mesothelial cells remain unclear. Here, we showed that the deleterious effects of nonfunctionalized MWCNTs on human mesothelial cells were associated with their diameter-dependent piercing of the cell membrane. Thin MWCNTs (diameter ~ 50 nm) with high crystallinity showed mesothelial cell membrane piercing and cytotoxicity in vitro and subsequent inflammogenicity and mesotheliomagenicity in vivo. In contrast, thick (diameter ~ 150 nm) or tangled (diameter ~ 2–20 nm) MWCNTs were less toxic, inflammogenic, and carcinogenic. Thin and thick MWCNTs similarly affected macrophages. Mesotheliomas induced by MWCNTs shared homozygous deletion of *Cdkn2a/2b* tumor suppressor genes, similar to mesotheliomas induced by asbestos. Thus, we propose that different degrees of direct mesothelial injury by thin and thick MWCNTs are responsible for the extent of inflammogenicity and carcinogenicity. This work suggests that control of the diameter of MWCNTs could reduce the potential hazard to human health.

environmental health | inflammation | nanotoxicology

Multiwalled carbon nanotubes (MWCNTs) (1) have received much interest since their discovery because of their unique physical and chemical properties (2). However, serious concerns have been raised that nanomaterials may induce malignant mesothelioma (3, 4), a cancer derived from mesothelial cells, which line somatic cavities. The similarity of these MWCNTs to asbestos fibers that are well known carcinogens for the mesothelium has been discussed (5–7).

The mechanism of fiber-induced carcinogenesis remains elusive. Currently, the interaction of fibers with cells may be divided into two distinct processes (7), direct effects of fibers on mesothelial cells (8–10) and indirect effects of fibers by inducing frustrated phagocytosis by macrophages (11), in which fiber length and rigidity are thought to be critical (12, 13). Rigid, durable fibers longer than 15 to 20 μm with a high aspect ratio have been proposed to be carcinogenic based on their indirect effects, which promote the continuous activation of macrophages (14–16). Indeed, long MWCNTs and long asbestos fibers induce frustrated phagocytosis and granuloma formation (17). This "length-dependent theory" has been recently reviewed (14).

With regard to the direct effects on the mesothelial tissue, previous studies have demonstrated the potential cytotoxicity of MWCNTs (18). However, critical factors that determine mesothelial cytotoxicity are still poorly understood. The direct interaction between MWCNTs and mesothelial cells appears to be a key event for the initiation of mesothelial carcinogenesis and for inducing inflammation (7, 19).

The morphological resemblance between MWCNTs and asbestos fibers has been emphasized. However, based on the variation in density, chemical composition, and surface reactivity, there should be multiple differences between nanotube toxicity and asbestos toxicity that would give us a clue to assist in the establishment of appropriate safety regulations and prevention of environmental health problems. To find such differences, we studied the direct interaction of MWCNTs with mesothelial cells in comparison with that of asbestos in the present study.

Results

Fiber Characteristics and Cell Lines. We used five different types of MWCNT grown in the vapor phase: NT50a was from Mitsui and NT50b, NT115, NT145, and NTtngl were from Showa Denko. NT50a, NT50b, NT115, and NT145 were named after their diameter in nanometers. NTtngl nanotubes were the thinnest MWCNTs used in this study and had a tangled conformation (Fig. 1*A*). Detailed information for all materials used is summarized in Table S1. We suspended MWCNTs in saline solution containing 0.5% BSA (henceforth A-saline solution). Three different asbestos fibers [chrysotile A (Chry), crocidolite (Cro), and amosite (Amo); Union for International Cancer Control] were used and were suspended in saline or A-saline solution. Two human mesothelial cell lines, MeT5A (SV40-transformed mesothelial cells) and E6/E7 and hTERT-immortalized human peritoneal mesothelial cells (HPMCs), were used. The HPMC culture was isolated and expanded according to an established protocol (20) with some modifications (21, 22) (*SI Materials and Methods*). Murine macrophages (RAW264.7) and canine kidney

Author contributions: H.N. and S.T. designed research; H.N., Y.O., S.H.C., N.M., Y. Yamashita, S.A., T.I., K.Y., Y. Yoshikawa, H.Y., L.J., H.O., Y.M., and H.S. performed research; Y. Yamashita, T.T., and G.I. contributed new reagents/analytic tools; H.N., S.A., Y. Yoshikawa, H.Y., Y.M., H.S., and S.T. analyzed data; and H.N., K.K., and S.T. wrote the paper.

The authors declare no conflict of interest.

This article is a PNAS Direct Submission.

[1]To whom correspondence should be addressed. E-mail: toyokuni@med.nagoya-u.ac.jp.

This article contains supporting information online at www.pnas.org/lookup/suppl/doi:10.1073/pnas.1110013108/-/DCSupplemental.

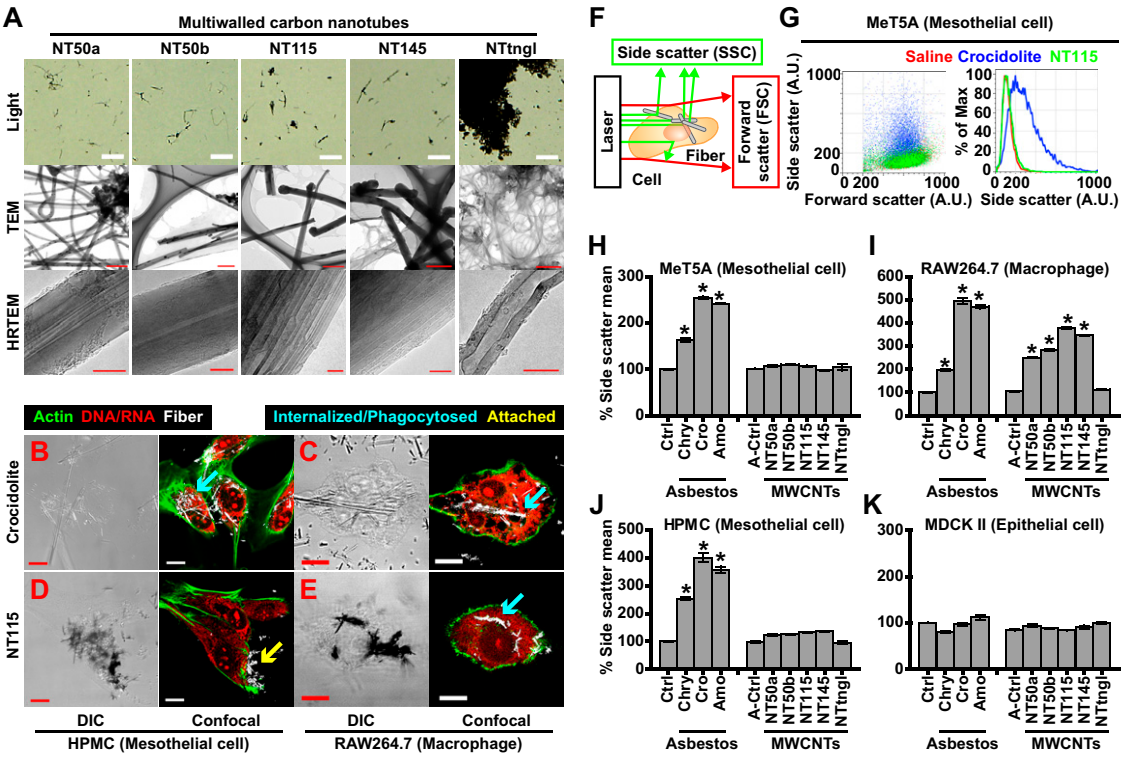

Fig. 1. Mesothelial cells did not phagocytose MWCNTs. (*A*) Optical and transmission EM (TEM) images and high-resolution (HR) Transmission EM images for five types of MWCNTs. Each carbon nanotube is named after its diameter (Fig. 2 and Table S1) except NTtngl, which stands for tangled NTs. High-resolution transmission EM images show the presence of graphite layers in the MWCNTs. (Scale bars: light microscopy, 20 μm; all transmission EM images except NTtngl, 500 nm; NTtngl transmission EM image, 200 nm; and high-resolution transmission EM images, 10 nm.) (*B* and *D*) Differential interference contrast and confocal Images of HPMCs show Cro internalization (blue arrow) and NT115 attachment (yellow arrow) after a 24-h incubation. (*C* and *E*) Images of RAW264.7 cells show internalization of both fibers (blue arrows). (*B–E*) Differential interference contrast images (*Left*) and confocal microscopy images (*Right*) after staining of the cells with Alexa 488-phalloidin (green) and propidium iodide (PI, red), indicate cytoskeletal actin and DNA/RNA, respectively. (Scale bars: *B–E*, 14 μm.) (*F*) A schematic showing the SSC and forward scatter (FSC) values for uptake of fibers. (*G*) *Left*: Dot plot of forward scatter and SSC values of MeT5A cells show a marked increase in SSC only upon incubation with Cro, but not with NT115. *Right*: Histogram shows SSC value of the image on the left. (*H–K*) Mean of the SSC value of each cell after a 3-h incubation with each fiber type (*$P < 0.001$; $n = 3$, mean ± SEM). *P* values were calculated between control (saline) and asbestos, or A-control (A-saline solution) and MWCNTs.

epithelial cells (MDCK II) were used as positive and negative controls, respectively.

Mesothelial Cells Did Not Internalize MWCNTs. We exposed two mesothelial cell lines, macrophages and epithelial cells, to 5 μg/cm^2 MWCNTs or 5 μg/cm^2 asbestos. After a 24-h incubation, we used confocal microscopy to detect the fibers (23) and found that HPMCs internalized Cro but not NT115, whereas macrophages phagocytosed both fibers (Fig. 1 *B–E*). NT115 fibers were found only attached to the surface of mesothelial cells (Fig. 1*D*). To quantitatively evaluate cell internalization, the side scatter (SSC) value in flow cytometry was used because it has been reported that fibers inside a cell increase the SSC value (24, 25) (Fig. 1*F* and Fig. S1*A*). The two mesothelial cell lines and macrophages showed a marked increase in SSC after a 3-h incubation with asbestos (Fig. 1 *G*, *H*, and *J*), consistent with previous reports (26, 27). However, MWCNTs differentially affected each cell line. Macrophages showed an increase in SSC after incubation with all types of MWCNTs except NTtngl (Fig. 1*I*), indicating that NTtngl was not phagocytosed by macrophages. Interestingly, the two mesothelial cell lines did not exhibit increased SSC after incubation with MWCNTs (Fig. 1 *G*, *H*, and *J*). These results were also confirmed by time-lapse microscopic analysis (Movies S1–S4). A slight increase in SSC was observed in HPMCs after incubation with MWCNTs because of the attachment of the fibers to the cells (Fig. 1 *D* and *J*). MDCK II epithelial cells showed no increase in SSC with any of the fibers used (Fig. 1*K*), indicating no internalization.

To further elucidate the internalization mechanism of Cro into mesothelial cells, we labeled rab5a (an early endosome marker) with GFP and actin with mCherry. Upon exposure to asbestos, HPMCs exhibited rab5a assembly at the periphery of Cro, whereas no rab5a concentration was observed after incubation with NT50a or NT145 (Fig. S1*B*), indicating that Cro fibers were actively internalized by mesothelial cells, but NT50a and NT145 were not. These data were also validated by using an inactive form of rab5a (28, 29) (Fig. S1*C*).

Inverse Correlation Between MWCNT Diameter and Mesothelial Cell Toxicity. Because mesothelial cells did not internalize MWCNTs, we suspected that the toxicity of MWCNTs would be limited because internalization of asbestos fibers has been shown to be important in asbestos-induced cell death (10, 19). We used three different assays (luminescence, light absorbance, and fluorescence) to evaluate cell viability, and the results were consistent among all the assays. Unexpectedly, different types of MWCNTs induced different levels of cytotoxicity in mesothelial cells. NT145 and NTtngl induced cytotoxicity to a limited extent, whereas NT50a was highly cytotoxic (Fig. 2*A*). We then found that the degree of cytotoxicity was inversely correlated with the mean diameter of dispersed MWCNTs (Fig. 2*B*).

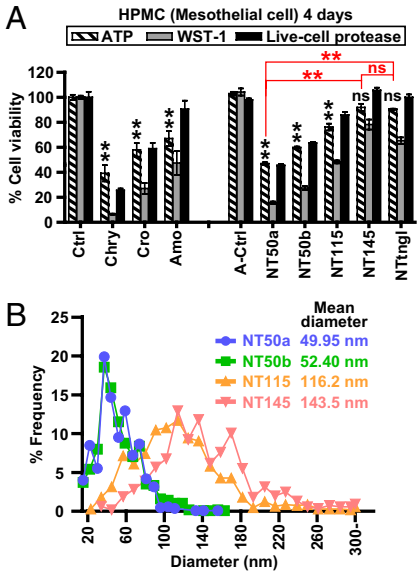

Fig. 2. Diameter of MWCNTs inversely correlated with mesothelial toxicity. (*A*) Cell viability assays of HPMCs after a 4-d incubation with each fiber at 5 μg/cm^2 show variable mesothelial cell cytotoxicity by MWCNTs. NT50a showed strong cytotoxicity against mesothelial cells, whereas NT145 and NTtngl did not. Ctrl, control. *P* values were calculated between control (saline) and asbestos or A-control (A-saline solution) and MWCNTs (n = 3, mean ± SEM; $^{**}P < 0.01$; ns, not significant). (*B*) Distribution of the diameters of MWCNTs.

Thin and Rigid MWCNTs Penetrated Plasma and Nuclear Membranes of Mesothelial Cells. Given that the diameter of dispersed MWCNTs was important in influencing mesothelial injury, we hypothesized that thin MWCNTs were cytotoxic by piercing the cell membrane, as the force to penetrate cell membranes has been found to be proportionally dependent on fiber diameter (30). For these studies, we defined internalization, phagocytosis, and piercing as follows: internalization as an active behavior of nonphagocytic cells (e.g., mesothelial cells) to engulf foreign materials, phagocytosis as an active process by phagocytes to engulf foreign materials, and piercing as an energy-independent penetration of cell membranes by fibrous materials that may or may not lead to translocation inside cells (depending on the type of material). After a 3-h incubation with fibers, HPMCs were fixed, embedded in Epon resin, and sliced into 80-nm or 500-nm ultrathin sections. After visualization by transmission EM, we classified Cro and MWCNTs as inside a cell/nucleus, crossing a cellular/nuclear membrane, or both. We found that NT50a nanotubes penetrated the plasma and nuclear membranes, whereas NT115 and NT145 did not (Fig. 3 *A*–*C*). Remarkably, the MWCNTs that pierced the membranes were not covered by vesicular membrane structures (Fig. 3*B*), indicating that the penetration occurred without active cellular processes, such as endocytosis or phagocytosis. In contrast, Cro was surrounded by vesicular structures (Fig. 3*B*). We concluded from these results that MWCNTs and asbestos enter mesothelial cells in a different manner.

Scanning EM was also used to observe localization of fibers that penetrated the plasma membrane or attached onto a cell surface (Fig. 3*D*). The thin dispersed MWCNTs (e.g., NT50a) were confirmed to pierce mesothelial membranes, whereas the thick dispersed MWCNTs (e.g., NT145) were unable to injure mesothelial cells. This diameter-dependent membrane piercing by fibers was specific to MWCNTs. In the case of Cro, even thicker fibers than NT145 were internalized (Fig. S2). The thinnest fiber (NTtngl) did not penetrate the cells because it formed bundled aggregates.

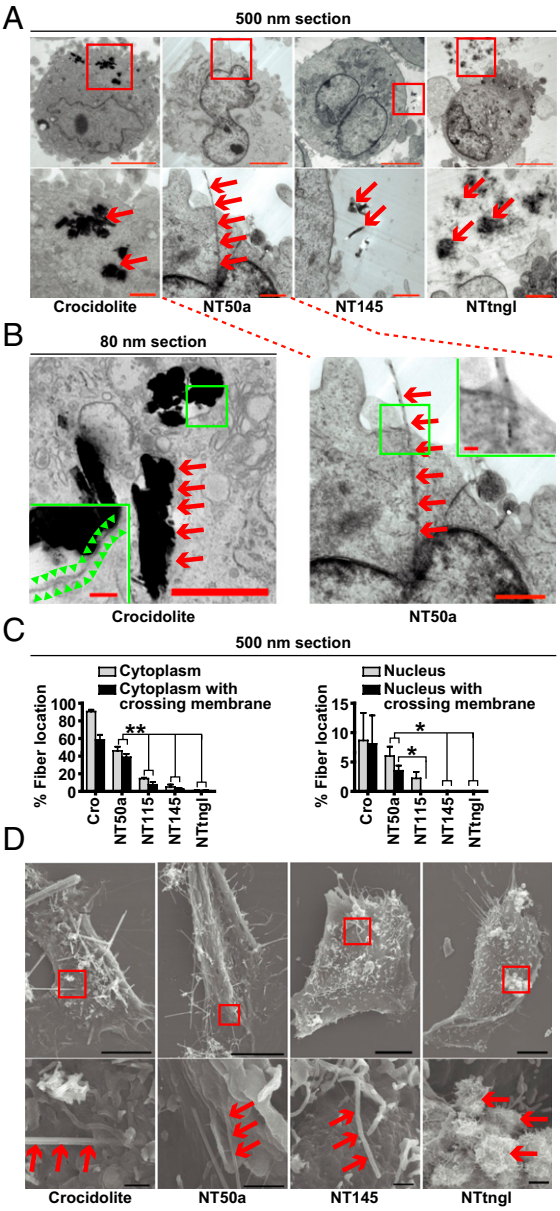

Fig. 3. Thin, dispersed MWCNTs with high crystallinity pierced mesothelial cells. (*A*) Representative transmission EM images of HPMCs after a 3-h incubation with indicated fibers. Ultrathin sections were prepared at a thickness of 500 nm. Squares (*Upper*) indicate insets (*Lower*). Cro was fully internalized. NT50a penetrated the mesothelial cell membrane, but NT145 and NTtngl did not (red arrow). (Scale bars: *Upper*, 10 μm; *Lower*, 1 μm.) (*B*) Cro was internalized and surrounded by a vesicular membrane structure (*Left*), whereas NT50a pierced the plasma membrane of the mesothelial cell without a vesicular structure surrounding the nanotubes (*Right*). We prepared 80-nm sections to show vesicular structure. Green arrowhead indicates vesicular structure. (Scale bars: 1 μm; *Insets*, 100 nm.) (*C*) Localization of fibers in transmission EM images (n = 3, mean ± SEM; $^{*}P < 0.05$ and $^{**}P < 0.01$). *P* values were calculated by Student's *t* test. (*D*) Representative scanning EM images of HPMCs after a 3-h incubation with indicated fibers.

Physicochemical Factors of MWCNTs Other Than Diameter Were Not the Primary Causes of Mesothelial Injury. Besides diameter, there could be multiple factors involved in MWCNT-induced toxicity. The distribution of length in each MWCNT type was very simi-

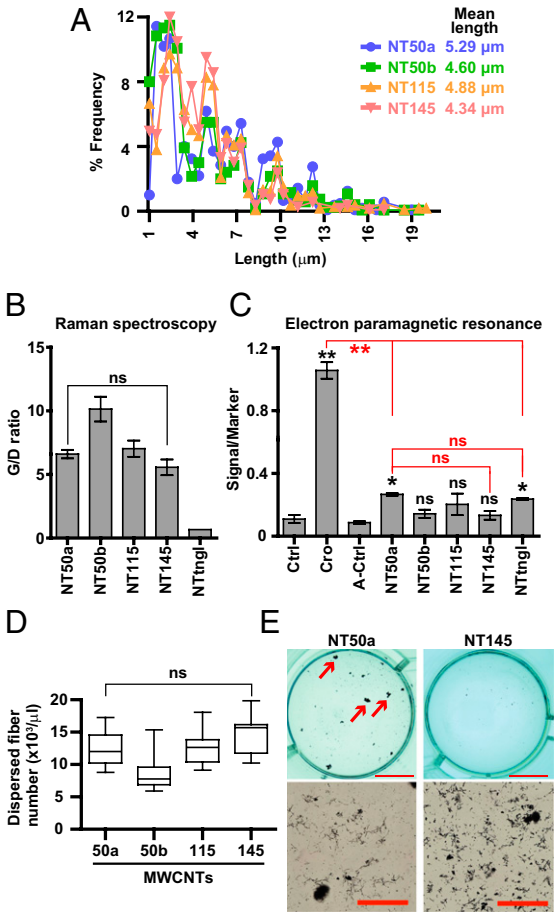

Fig. 4. Other factors, including length, structural defects, free radical generation, and difference in number of fibers, were not the primary causes of mesothelial cell cytotoxicity by thin, dispersed MWCNTs with high crystallinity. (*A*) Distribution of the lengths of MWCNTs. (*B*) Graphite/defect (G/D) ratio shows no significant difference in defect abundance between NT50a and NT145. (*C*) EPR shows that NT50a and NTtngl produce hydroxyl radicals in the presence of hydrogen peroxide, whereas NT145 does not. Cro was most potent in free radical generation. *P* values were calculated between control (saline) and asbestos or A-control (A-saline) and MWCNTs. (*D*) Number of dispersed fibers in 0.5 mg/mL fiber suspensions. (*E*) Macroscopic and microscopic images of NT50a and NT145 suspensions under experimental conditions (5 μg/cm^2). Arrows indicate nanotube aggregation, which greatly reduces the suspension of dispersed fibers. (Scale bars: *Upper*, 10 mm; *Lower*, 100 μm.) *P* values (*$P < 0.05$ and **$P < 0.01$; ns, not significant) were determined by one-way ANOVA with post-hoc Dunnett test (*C*) or Tukey test (*B* and *D*).

lar, and the majority of the nanotubes were less than 10 μm in length (Fig. 4*A*). Lengths greater than 10 μm have been shown to promote increased toxicological reactivity (31). We performed Raman spectroscopy and found no significant difference between NT50a and NT145 in the relative amounts of structural defects (32, 33) (Fig. 4*B*). We measured free radical generation (34) by electron paramagnetic resonance and soluble metals (35) by inductively coupled plasma MS. The results showed no significant difference between NT50a and NTtngl (Fig. 4*C* and Fig. S3*A*), indicating that contaminating metals, at least when they are outside cells, do not play a central role in the current toxicity assays.

We tested the cytotoxicity of MWCNTs based on their weight. To exclude the possibility that the thin MWCNTs were toxic just because the number of fibers was greater than in the thick MWCNTs, we assessed the number of dispersed fibers in suspension. There was no significant difference in the number of dispersed fibers between NT50a and NT145 (Fig. 4*D*). This is because NT50a nanotubes were likely to form agglomerates because of their high aspect ratio, leading to a decrease in the number of dispersed fibers in suspension (Fig. 4*E*).

The large surface area of MWCNTs is also considered to be an important factor in toxicology because it depletes nutrients and growth factors in culture medium, resulting in cell death from starvation (36). We tested whether this phenomenon contributed to cellular toxicity by saturating the surface area with serum proteins. The serum-treated NT50a was still highly cytotoxic, whereas NT145 did not cause cell death (Fig. S3*B*). We also analyzed the profile of protein absorption on each fiber (37), but there was no significant difference between NT50a and NT145 (Fig. S3 *C* and *D*). Accordingly, surface area was not the primary cause of mesothelial injury in the present study.

Taken together, length (largely <10 μm), structural defects, free radical generation, difference in number of fibers, contaminating metals, and surface area were not considered to be the primary causes of the direct cytotoxicity of NT50a toward mesothelial cells. Instead, our studies demonstrated that the diameter of MWCNTs was one of the critical factors responsible for mesothelial cell injury.

Thin and Rigid MWCNTs Induced Severe Chronic Inflammation. To study the effects of each MWCNT type in vivo, rats were killed 1 mo after an i.p. injection with 1 or 5 mg of NT50a, NT145, or NTtngl. Distinct macroscopic differences were observed among the three nanotube types. NT50a caused severe fibrous peritonitis and induced dull edge in the liver. In contrast, NT145 and NTtngl did not cause such effects, even at five times higher concentration (Fig. 5*A* and Fig. S4*A*). All MWCNTs administered to rats were phagocytosed by macrophages, and local granuloma formation was observed (Fig. S4*D*). Notably, rats treated with NT145 and NTtngl showed negligible fibrosis surrounding fiber deposition, in contrast to rats administered NT50a (Fig. 5 *B* and *C* and Fig. S4 *B* and *C*). Because fibrosis was observed around each i.p. organ regardless of MWCNT deposition, we calculated a fibrosis index and confirmed that NT50a was the most potent inducer of fibrotic inflammation (Fig. 5*D*). We observed iron deposition in NT50a-induced fibrotic tissue, which was derived from the rat organs because NT50a deposition itself did not react to Perls' iron staining (Fig. S4*E*). Furthermore, the proliferation of mesothelial cells was observed only in rats treated with NT50a (Fig. S4*F*).

Inflammation is a systemic response to foreign bodies or wounds and is driven by various stimuli, such as cytokines and necrotic cell debris. In the abdominal cavity, there are resident macrophages as well as mesothelial cells surrounding the cavity. Here, we hypothesized that the difference in the extent of inflammation induced by NT50a and NT145 was caused by differences in the ability to induce direct mesothelial injury because all types of MWCNT affected macrophages similarly in terms of cytotoxic effects and inflammatory responses (Fig. 5 *E* and *F*). Indeed, mesothelial injury caused by asbestos can induce inflammation as previously shown (19).

Thin and Rigid MWCNTs Induced Frequent and Early Mesothelial Carcinogenesis in Rats. Finally, we tested the carcinogenicity of each MWCNT type by i.p. injection into rats to allow MWCNTs to directly interact with mesothelial cells immediately after administration. We injected 1 mL of MWCNT suspension into 6-wk-old rats twice with a 1-wk interval and observed them for 1 y. We used total doses of 1 mg or 10 mg per animal in addition to a special group of rats injected with NT50a, referred to as NT50a(-agg*), meaning no aggregation. We prepared this special group to eliminate the agglomeration activity of NT50a and equalize the number of fibers to 1 mg NT145. We centrifuged 0.5 mg/mL

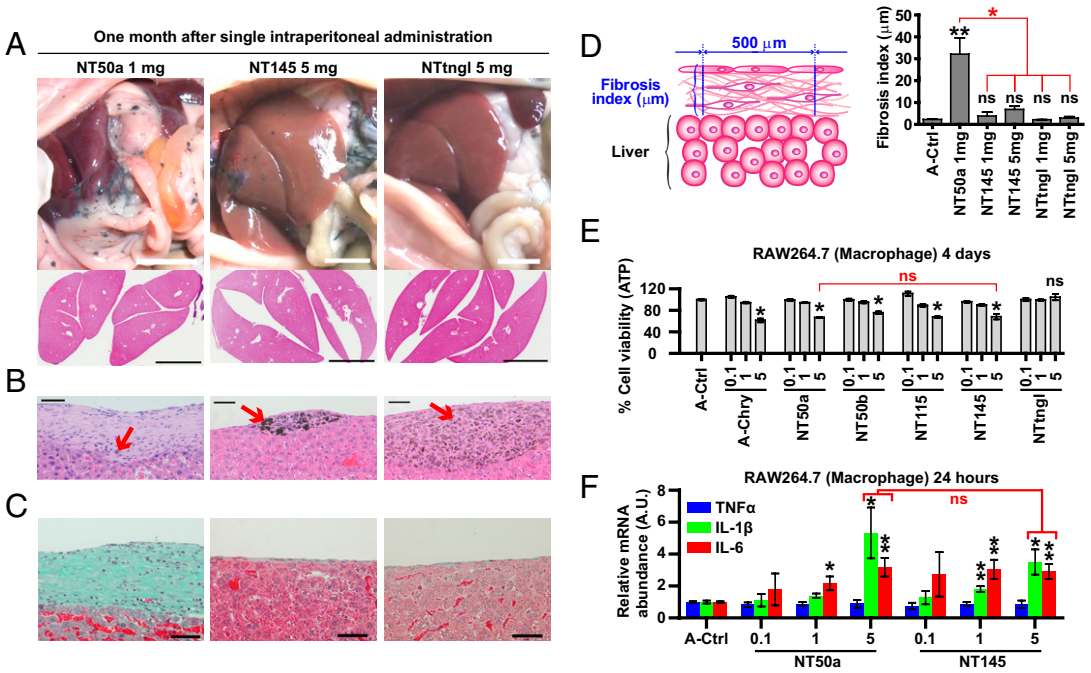

Fig. 5. Thin, dispersed MWCNTs with high crystallinity caused severe fibrotic peritonitis in rats, although affected macrophages in vitro similarly compared with the other MWCNTs. (*A–C*) Macroscopic and microscopic images of rat organs 1 mo after a single i.p. injection of 1 mg NT50a (*Left*), 5 mg NT145 (*Middle*), or 5 mg NTtngl (*Right*). (*A*) Macroscopic images of i.p. organs immediately after dissection (*Top*). Low-power view of H&E-stained livers show an altered dull edge (*Lower Left*). (Scale bar: 1 cm.) (*B*) Microscopic images of the liver surface show the deposition of fibers (arrow) and various fibrotic responses around fibers. (Scale bars: 50 μm.) (*C*) Masson trichrome stain showing abundant light green collagen (*Left*). (Scale bars: 50 μm.) (*D*) Fibrosis index was calculated by measuring the distance from the entire outer surface of the liver to the mesothelium at intervals of 500 μm (*Left*). Fibrosis index shows that NT50a induced the strongest fibrotic inflammation [*Right*; $n = 3–6$, mean ± SEM; $^*P < 0.05$; ns, not significant between A-control (A-saline) and MWCNT]. (*E*) Cell viability assays of macrophages (RAW264.7) after a 4-d incubation with each fiber at indicated concentrations (0.1, 1, or 5 μg/cm^2) show that there was no significant difference in cytotoxic effects between NT50a and NT145. (*F*) Macrophages showed increased mRNA levels of IL-1β and IL-6 after a 24-h incubation with NT50a and NT145 at 5 μg/cm^2, and there was no significant difference between NT50a and NT145 for mRNA of inflammatory cytokines ($n = 3–6$, mean ± SEM; $^*P < 0.05$ and $^{**}P < 0.01$; ns, not significant). *P* values were determined by one-way ANOVA with post-hoc Tukey test (*D* and *E*) or by Student's *t* test (*F*).

NT50a and collected the supernatant, which we named NT50a (-agg), to eliminate agglomerate (Fig. 6*A*). We doubled the concentration of NT50a (1 mg/mL) for centrifugation to equalize the number of dispersed fibers in the NT50a(-agg*) suspension and the 0.5 mg/mL NT145 suspension (Fig. 6*B*). For the other dosing, the 10-mg injection was a relatively high dose, and nearly half the rats died within several days (Table S2). Consequently, we used the remaining animals as the 10-mg injection group. None of the rats administered 1 mg of MWCNTs died immediately after injection. Rats were killed when bloody ascites or weight loss was prominent or after 1 y from the initial administration.

Injections with NT50a(-agg*) or 1 mg of NT50a induced malignant mesothelioma with a higher frequency and earlier progression than injections with 1 mg of NT145 and 10 mg of NTtngl. Representative images of mesothelioma are shown in Fig. 6 *C* and *D*. The survival curve and overall tumor incidence showed that NT50a(-agg*) and 1 mg of NT50a were more carcinogenic than 1 mg of NT145 (Fig. 6 *E* and *F*). Even in the same group, tumor progression and histologic findings were variable (Fig. S5 and Table S2). Notably, most of the tumors induced by MWCNTs exhibited sarcomatoid histology (epithelioid, 0.9%; biphasic, 12.1%; sarcomatoid, 86.0%; not determined, 0.9%), indicating that the mesotheliomas induced by MWCNTs were more aggressive in nature. To study the genomic alteration of the tumors, we performed an array-based comparative genomic hybridization (CGH) analysis and found that there were homozygous deletions of *Cdkn2a/2b* in almost all the tumors tested (Fig. 7 and Fig. S6), which is one of the most common genetic aberrations found in mesotheliomas in both humans (38, 39) and rodents (40, 41). There were numerous other genomic amplifications and deletions, but they were not consistent among tumors.

Discussion

We investigated five different types of MWCNTs and their direct effect on mesothelial cells in comparison with three types of asbestos fibers by studying cellular internalization, injury, inflammogenicity, and carcinogenicity (as summarized in Fig. 8 and Table S1). We focused on how MWCNTs differed from asbestos, not on how MWCNTs behaved like asbestos. We demonstrated that MWCNTs directly pierced mesothelial plasma and nuclear membranes, whereas asbestos fibers were internalized by mesothelial cells via encapsulation by vesicular membranous structures. Because of this difference, thick MWCNTs (e.g., NT145) were less likely to pierce mesothelial cells than thin MWCNTs (e.g., NT50a), even though Cro, which is even thicker than NT145, was easily internalized by the cells. Therefore, although MWCNTs and asbestos both share needle-like structures and have high durability, they do not necessarily enter mesothelial cells in the same way. Thus, nanotube toxicology should be evaluated differently than asbestos toxicology under certain conditions.

Surface characteristics of MWCNTs, such as functionalization, degree of hydrophobicity, and protein modification, are thought to be important in internalization events (31, 42–44). The present study used pristine MWCNTs without any chemical functionalization and suspended MWCNTs in saline solution containing albumin as previously described (17). To determine possible environmental or toxicological risks of MWCNTs, the use of pristine MWCNTs was considered more appropriate because chemical functionalization of bulk MWCNTs is unrealistic and has

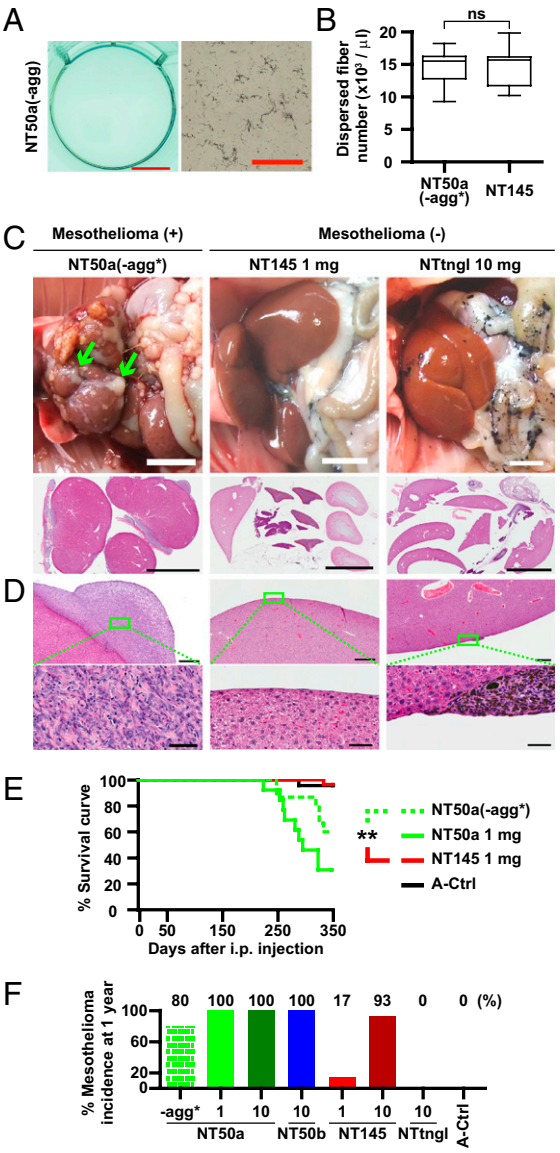

Fig. 6. Thin, dispersed MWCNTs with high crystallinity had higher mesotheliomagenicity than thick MWCNTs when injected intraperitoneally into rats. (*A*) Macroscopic and microscopic images of NT50a(-agg). NT50a(-agg) consisted of the supernatant of the original NT50a suspension after centrifugation. No agglomeration can be seen (compare vs. Fig. 4*E*). (Scale bars: *Left*, 10 mm; *Right*, 100 μm.) (*B*) NT50a(-agg*) had twice as many fibers in suspension as NT50a(-agg). The number of dispersed fibers in NT50a(-agg*) and NT145 was almost the same (ns, not significant). The text provides further details. (*C*) Macroscopic images of i.p. organs immediately after dissection (*Upper*). Mesothelioma covers liver surface (*Upper Left*). Low-power view of H&E-stained livers shows malignant mesothelioma (*Lower Left*) or absence of mesothelioma (*Lower Middle*, *Lower Right*). (Scale bars: 1 cm.) (*D*) Microscopic images of the liver surface show mesothelioma (*Left*). Granuloma is seen (*Right*), and squares (*Upper*) indicate insets (*Lower*). (Scale bars: *Upper*, 500 μm; *Lower*, 50 μm.) (*E*) Survival curve of rats injected with MWCNTs and vehicle control shows that there was significant difference in mesotheliomagenicity between NT50a (-agg*) and NT145 (**$P < 0.01$). (*F*) Overall tumor probability induced by each fiber during the 1-y observation period. The number below the *x* axis indicates the amount of injected fibers [in mg; $n = 15$ in NT50a(-agg*), $n = 13$ in 1 mg NT50a, $n = 43$ in 10 mg NT50a, $n = 6$ in 10 mg NT50b, $n = 29$ in 1 mg NT145, $n = 30$ in 10 mg NT145, $n = 15$ in 10 mg NTtngl, and $n = 23$ in A-saline solution (A-Ctrl)]. Table S2 includes the numbers of rats used and histology of mesothelioma. *P* values were determined by Student's *t* test (*B*) or by log-rank test (*E*).

been shown to significantly improve the toxicological profile of nanotubes (45). Albumin was used as a dispersing medium for

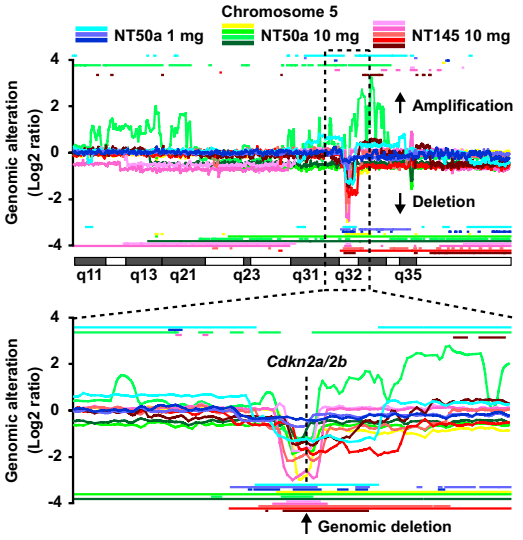

Fig. 7. *Cdkn2a/2b* was homozygously deleted in MWCNT-induced mesothelioma of rats. Array-based CGH analysis of mesotheliomas shows that the genomic locus, *Cdkn2a/2b*, was homozygously or heterozygously deleted in all mesothelioma cases tested. Horizontal lines above and below the CGH ratio curve were delineated based on *z*-score (*Materials and Methods*), indicating amplification and deletion of the indicated loci, respectively. At the *Cdkn2a/2b* locus, all tumors have horizontal lines below the CGH curve and thus have genomic deletion. Fig. S6 shows signal intensity and extent of genomic deletion at the *Cdkn2a/2b* locus.

MWCNTs because it is abundant in cell culture media supplemented with FBS as well as in serum and pleural fluid in vivo (46). We also evaluated the profile of protein adsorption on the MWCNTs (Fig. S3 *C* and *D*), but there were no significant differences found between the MWCNTs.

We hypothesized that the diameter of MWCNTs played a major role in determining whether the nanotubes would be able to directly pierce cell membranes. A similar idea was suggested by Lacerda et al., who determined that MWCNTs pierced and directly translocated through cell membranes in an energy-independent manner (47); Vakarelski et al. showed that thin MWCNTs penetrated living cell membranes with minimal required force (i.e., energy) (30). We found that nanotube diameter critically determined whether MWCNTs led to increased risk of cytotoxicity after direct interaction, penetration, or injury of mesothelial cells. The exact mechanism of penetration of mesothelial cells by MWCNTs and the way in which membrane piercing by MWCNTs causes toxicity still remains unknown. Regarding the longitudinal dimension (i.e., length) of MWCNTs, significantly shorter MWCNTs have been previously reported to be nontoxic (42), whereas significantly longer MWCNTs compared with the ones used in the present study have been shown to be inflammogenic (14). The MWCNTs used in our study affected macrophages to the same extent (Fig. 5 *E* and *F*). Because length is an important factor in inducing macrophage activation (14, 16), the lack of difference in macrophage activation among each MWCNT type confirmed the evenness of fiber length and the similarity in mean length (Fig. 4*A*). Although length, contaminating metals, structural defects, and protein adsorption may be involved in cellular toxicity induced by penetrating MWCNTs, we confirmed here that these factors were not the primary causes of the difference in observed cytotoxicity. Notably, we showed that crystallinity, which determines MWCNT sharpness and rigidity, was an important structural feature because tangled MWCNTs, even though they were the thinnest (i.e., have the smallest diameter) of the nanotubes used, did not pierce mesothelial membranes or induce mesothelioma in rats, which is

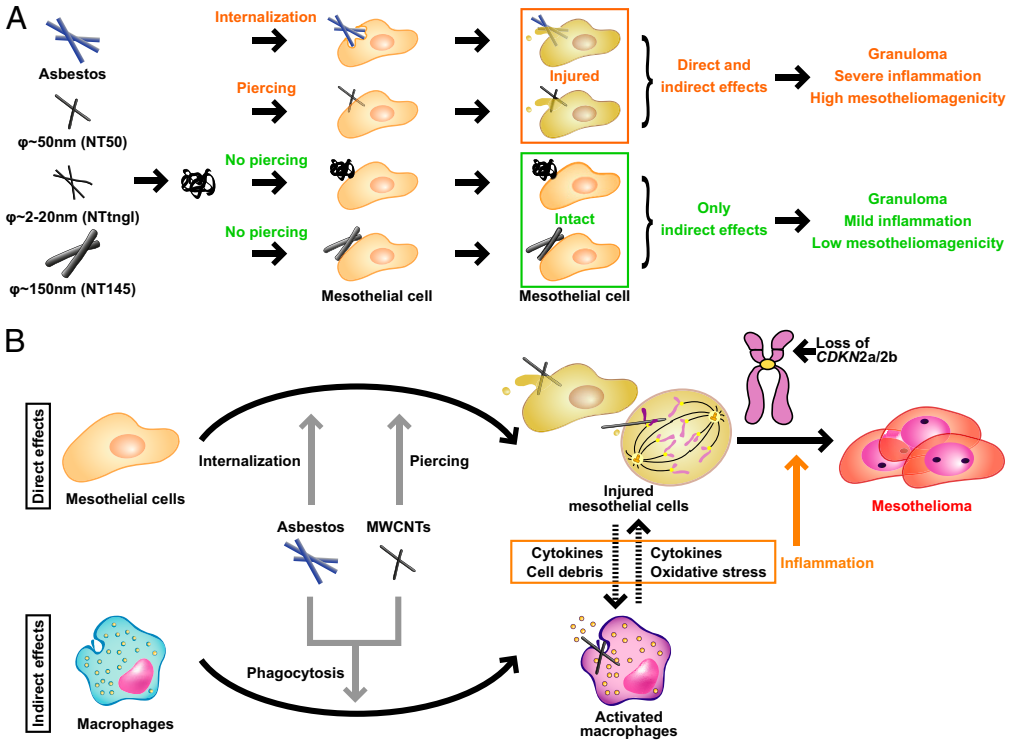

Fig. 8. Schematic of the effect of different MWCNTs on mesothelial cells. (*A*) The present study shows that asbestos and thin, dispersed MWCNTs with high crystallinity (diameter~ 50 nm; .e.g., NT50a) penetrate mesothelial cells and further induce cell injury. However, aggregative MWCNTs (diameter ~ 2–20 nm; e.g., NTtngl) and thick MWCNTs (diameter ~ 150 nm; e.g., NT145) do not penetrate mesothelial cells, and thus there is no cell injury, which may explain the difference in the carcinogenicity between thin and thick MWCNTs. (*B*) Current schematic for mechanisms of mesotheliomagenesis focused on mesothelial injury and macrophage activation. Interplay of these two factors may lead to persistent inflammation and subsequent mesotheliomagenesis.

in agreement with previously reported studies that used similar material (18, 48).

In the mesotheliomagenesis experiment, we used several doses of MWCNTs, including 1 mg and 10 mg. However, we would like to focus on the carcinogenicity of NT50a(-agg*) compared with that of 1 mg of NT145 because these two fiber suspensions contained nearly the same numbers of dispersed fibers (Fig. 6*B*) and both lacked agglomerates (Figs. 4*E* and 6*A*). We used the 10-mg injection group to avoid false-negative results in the NT145-injected group. Fortunately, we could perform array CGH analysis of mesothelioma samples from the 10-mg NT145 group, but not from the 1-mg NT145 group, because of the low incidence of mesothelioma. Thus, the present study demonstrated a profiling of genetic alterations in the mesothelium following long-term exposure to carbon nanotubes, revealing a common mechanism of mesotheliomagenesis (homozygous deletion of *Cdkn2a/2b*) in MWCNTs (NT50a and NT145) and asbestos (40, 41).

The shorter latency period of mesothelioma in MWCNT-injected rats than in asbestos-injected rats is reported in the literature (3, 4). The temporal disparity in mesotheliomagenesis may come from differences between the two fiber types, including how they injure mesothelial cells. Here, we demonstrated that MWCNTs behaved differently than asbestos fibers against mesothelial cells. Both thin MWCNTs with high crystallinity and asbestos fibers should induce the main two events in mesotheliomagenesis, mesothelial injury and macrophage activation. However, we found that the mechanism of mesothelial injury was different. This distinctness may partially explain the question above. For example, it is possible that MWCNTs that are located in the cytoplasm and are uncovered by membranes would be more likely to injure chromosomes during mitosis than asbestos fibers surrounded by membranous structures, resulting in a difference in the progression of mesothelioma. It is unknown how genetic aberrations are introduced into mesothelial cells by fibers, although we have several hypotheses, including free radical generation, mitotic disturbance, molecule adsorption, and inflammation (7, 49). Notably, the entry of fibers into mesothelial cells was associated with all these mechanisms. Indeed, there was a large difference in the extent of fibrotic inflammation between groups injected with thin or thick MWCNTs (Fig. 5 *A–D*) but no difference in the activation of and toxicity to macrophages (Fig. 5 *E* and *F*), which indicates the involvement of mesothelial injury in inflammation. The interplay of mesothelial injury and macrophage activation was previously reviewed elsewhere (7). In brief, mesothelial cell injury per se can activate macrophages and neutrophils and thus induce inflammation (50), which would explain why thin MWCNTs were more inflammogenic and carcinogenic than thick MWCNTs.

Our previous findings have shown that the loss of *Cdkn2a/2b* occurs in sarcomatoid mesothelioma induced by iron overload without fibers (51), but the tumors developed 2 y after injection, and the nature of the tumors was less aggressive. This rat model suggests that free radical generation inside the rat peritoneal cavity is sufficient to induce mesothelioma with the same genetic features as asbestos-induced mesothelioma. However, when comparing the progression of fiber-induced mesothelioma with iron overload-induced mesothelioma, there should be factors specific to fibers involved in mesotheliomagenesis that exacerbate the tumor initiation and growth.

There are some limitations to the present study. As in various other studies, we used the i.p. model of mesothelial exposure. Thus, a careful consideration of the multiple factors involved in fiber translocation from the airways to the pleura is important before conclusive assessments of the health risks posed by inhaled MWCNTs as carcinogens can be reached.

Most previously reported studies focus mainly on the length of MWCNTs in inflammogenicity and carcinogenicity (14, 31), based on the observation that long (>15–20 μm), biopersistent fibers induce frustrated phagocytosis. Even though such hypotheses are certainly useful, they do not offer a complete explanation of the complex mechanisms leading to mesotheliomagenesis. Our results suggested that direct mesothelial injury was crucial in inducing carcinogenesis with the same genetic signature as that of asbestos in a rat i.p. exposure model. Furthermore, we found that the thin diameter of nonfunctionalized MWCNTs in combination with high crystallinity resulted in rigid, needle-shaped nanomaterials that caused direct injury to mesothelial cells and presented a risk for induction of mesothelioma. In general, this study and others have helped instruct the ways in which MWCNTs should be designed (i.e., as short, flexible, thick, and chemically functionalized as possible) to be less biologically reactive and more prone to biodegradation. Further investigation is warranted to elucidate the effect of different types of nanotubes on long-term carcinogenesis and the detailed genetic cascades involved.

Materials and Methods

Materials. Five types of vapor-grown MWCNTs were donated. NT50a (MWNT-7, lot 061220–02) was obtained from Mitsui, and NT50b, NT115, NT145, and NTtngl were obtained from Showa Denko (Table S1). Three types of asbestos (Chry, Cro, and Amo) were obtained from the Union for International Cancer Control. The plasmids, mCherry-actin and EGFP-actin, were provided by Kozo Kaibuchi (Nagoya University, Nagoya, Japan) and Roger Y. Tsien (University of California, San Diego, La Jolla, CA). Plasmids with the WT and inactive form (S34N) of rab5a were kind gifts from Mitsunori Fukuda (Tohoku University, Tohoku, Japan). All rats were Fischer 344/Brown Norway F1 hybrids. Fischer 344 female rats and Brown Norway male rats were purchased from Charles River Japan. The animal experiment committee of Nagoya University Graduate School of Medicine approved these animal experiments. The MeT5A and RAW264.7 cell lines were obtained from the American Type Culture Collection. The MDCK II cell line was provided by Kozo Kaibuchi (Nagoya University, Nagoya, Japan). The HPMC line was established as described in *SI Materials and Methods*.

Detection of Cellular Uptake of Fibers. We grew cells at a density of 1×10^4 cells/cm^2 at 1 d before the addition of each fiber. In each experiment, 0.5 mg/mL fibers were added to the culture medium to a final concentration of 5 μg/cm^2. We used an LSM5PASCAL microscope (Zeiss) to obtain confocal images. Cells were fixed with 4% paraformaldehyde 24 h after the addition of the fibers and stained with Alexa 488-phalloidin (Invitrogen) and propidium iodide without RNase to stain the cytosol and nucleus at the same time. Fibers were detected with reflected or scattered laser light. For flow cytometry analysis, cells were collected 3 h after the addition of fibers (FACSCalibur; BD Biosciences).

Cell Viability Assays. We grew cells at a density of 3×10^3 cells/cm^2 for MeT5A cells and HPMCs and at 3×10^4 cells/cm^2 for RAW264.7 macrophages 24 h before the addition of the fibers (final concentration, 5 μg/cm^2). Four days after fiber addition, the following three types of live cell assays were performed: the live cell luminescence ATP detection assay (Cell Titer-Glo; Promega), the light absorbance mitochondrial activity assay (WST-1, Roche), and the fluorescence live-cell caspase activity assay (MultiTox-Fluor; Promega).

In Vivo Chronic Inflammation Assays. To observe the chronic phase, 6-wk-old male rats were injected with 1 mL of 1 mg/mL NT50a or 1 mL of 1 or 5 mg/mL NT145 or NTtngl. Tissues were harvested after 1 mo. We used three to six rats in each group. Paraffin-embedded tissues were subjected to H&E, Masson trichrome, or Perls' iron staining. Podoplanin (T-20; Santa Cruz Biotechnology) immunohistochemistry was performed as previously reported (52) to identify mesothelial cells. Fibrosis index was calculated by measuring the distance from the outer surface of the liver to the mesothelium at intervals of 500 μm. The measurement was made on a digital slide taken by Scanscope (Aperio Technologies).

Mesotheliomagenesis in Rats. Six-week-old male and female rats were injected with 1 mL of 0.5 or 5 mg/mL of the MWCNT suspension or 1 mL of NT50a(-agg*) twice with a 1-wk interval. NT50a(-agg*) consisted of the supernatant of 1 mg/mL NT50a after centrifugation at 2,200 × *g* for 10 s. We used 1 mg/mL of the NT50a suspension because the supernatant of the centrifuged 0.5 mg/mL NT50a suspension, NT50a(-agg), contained nearly half the number of fibers as 0.5 mg/mL NT145. NT50a(-agg*) contained no agglomerate and had approximately the same number of dispersed fibers as 0.5 mg/mL NT145. Thus, in the NT50a(-agg*) and 1 mg NT145 groups, rats were injected with almost the same number of fibers. Rats were killed when bloody ascites or weight loss was prominent. Rats that did not exhibit this phenotype were killed after approximately 1 y (350 d) had passed from the initial injection of MWCNTs. The cumulative probability of death was calculated for each group according to the Kaplan–Meier method and compared by using the log-rank test.

Array-Based CGH Analysis. We performed array-based CGH with a Rat Genome CGH Microarray 4x180K (G4841A; Agilent Technologies), as described in the Agilent Oligonucleotide Array-based CGH for Genomic DNA Analysis Protocol, version 6.2. For each array, a normal kidney was used as a reference and labeled with Cy-3. Samples of interest were labeled with Cy-5. Three, four, and five cases of mesothelioma that were induced by 1 mg NT50a, 10 mg NT50a, and 10 mg NT145, respectively, were assessed, and the results were analyzed with the Agilent Genomic Workbench Standard Edition (version 5.0). We identified regions of copy number alteration based on the *z*-score (threshold, 3.0). Centralization was performed with a threshold of 6.0 and bin size of 10. Genomic positions were based on the University of California, Santa Cruz, November 2004 rat reference sequence (rn4). We calculated moving averages of the signal log ratio with a window size of 0.5 Mb. We determined that all of the tumors have genomic deletion at *Cdkn2a/2b* because of the results of the chromosomal aberration analysis based on the *z*-score. Then, the extent of genomic deletion, namely whether it was homozygous or heterozygous, was determined by the value of y at the locus. We determined that the mesothelioma samples, whose signal intensity at the *Cdkn2a/2b* locus was largely lower than −1, had homozygous deletion of the gene (Fig. S6).

Statistics. All experiments were performed in triplicate. Data are expressed as mean values ± SEM. All statistics except the survival curve were calculated by using a one-way ANOVA with a post-hoc Tukey test, a one-way ANOVA with a post-hoc Dunnett test, or a Student's *t* test. The cumulative probability of death was compared by using a log-rank test. All statistics were calculated with Prism 5 software (GraphPad).

ACKNOWLEDGMENTS. We thank Midori Tanaka (Kyoto University) for schematics; Atsushi Enomoto, Takuya Kato (Nagoya University), and Shigekazu Nagata (Kyoto University) for comments on the manuscript; Takashi Watanabe (Nagoya University) for technical advice; and Yoshikazu Fujita and Ikuyo Mizuguchi (Division for Medical Research Engineering, Nagoya University Graduate School of Medicine) for technical support. This study was supported by a Long-range Research Initiative Grant from the Japan Chemical Industry Association; Princess Takamatsu Cancer Research Fund Grant 10-24213; grant-in-aid for Cancer Research from the Ministry of Health, Labor and Welfare of Japan; grant-in-aid from the Ministry of Education, Culture, Sports, Science and Technology (MEXT) of Japan; a MEXT Special Coordination Funds for Promoting Science and Technology Grant; a grant from the Takeda Science Foundation; and grant-in-aid from the Japan Society for the Promotion of Science Fellows. K.K. is the recipient of a professorial fellowship from the Japan Society for the Promotion of Science.

1. Iijima S (1991) Helical microtubules of graphitic carbon. *Nature* 354:56–58.
2. Thayer AM (2007) Carbon nanotubes by the metric ton. *Chem Eng News* 85: 29.
3. Sakamoto Y, et al. (2009) Induction of mesothelioma by a single intrascrotal administration of multi-wall carbon nanotube in intact male Fischer 344 rats. *J Toxicol Sci* 34:65–76.
4. Takagi A, et al. (2008) Induction of mesothelioma in p53+/- mouse by intraperitoneal application of multi-wall carbon nanotube. *J Toxicol Sci* 33:105–116.
5. Donaldson K, Poland CA (2009) Nanotoxicology: New insights into nanotubes. *Nat Nanotechnol* 4:708–710.
6. Jaurand MC, Renier A, Daubriac J (2009) Mesothelioma: Do asbestos and carbon nanotubes pose the same health risk? *Part Fibre Toxicol* 6:16.
7. Nagai H, Toyokuni S (2010) Biopersistent fiber-induced inflammation and carcinogenesis: lessons learned from asbestos toward safety of fibrous nanomaterials. *Arch Biochem Biophys* 502:1–7.
8. Hei TK, Piao CQ, He ZY, Vannais D, Waldren CA (1992) Chrysotile fiber is a strong mutagen in mammalian cells. *Cancer Res* 52:6305–6309.
9. Ramos-Nino ME, Timblin CR, Mossman BT (2002) Mesothelial cell transformation requires increased AP-1 binding activity and ERK-dependent Fra-1 expression. *Cancer Res* 62:6065–6069.

10. Yang H, et al. (2006) TNF-alpha inhibits asbestos-induced cytotoxicity via a NF-kappaB-dependent pathway, a possible mechanism for asbestos-induced oncogenesis. *Proc Natl Acad Sci USA* 103:10397–10402.
11. Dostert C, et al. (2008) Innate immune activation through Nalp3 inflammasome sensing of asbestos and silica. *Science* 320:674–677.
12. Donaldson K, Brown GM, Brown DM, Bolton RE, Davis JM (1989) Inflammation generating potential of long and short fibre amosite asbestos samples. *Br J Ind Med* 46:271–276.
13. Oberdörster G (2002) Toxicokinetics and effects of fibrous and nonfibrous particles. *Inhal Toxicol* 14:29–56.
14. Donaldson K, Murphy FA, Duffin R, Poland CA (2010) Asbestos, carbon nanotubes and the pleural mesothelium: A review of the hypothesis regarding the role of long fibre retention in the parietal pleura, inflammation and mesothelioma. *Part Fibre Toxicol* 7:5.
15. Stanton MF, et al. (1981) Relation of particle dimension to carcinogenicity in amphibole asbestoses and other fibrous minerals. *J Natl Cancer Inst* 67:965–975.
16. Ye J, et al. (1999) Critical role of glass fiber length in TNF-alpha production and transcription factor activation in macrophages. *Am J Physiol* 276:L426–L434.
17. Poland CA, et al. (2008) Carbon nanotubes introduced into the abdominal cavity of mice show asbestos-like pathogenicity in a pilot study. *Nat Nanotechnol* 3:423–428.
18. Tabet L, et al. (2009) Adverse effects of industrial multiwalled carbon nanotubes on human pulmonary cells. *J Toxicol Environ Health A* 72:60–73.
19. Yang H, et al. (2010) Programmed necrosis induced by asbestos in human mesothelial cells causes high-mobility group box 1 protein release and resultant inflammation. *Proc Natl Acad Sci USA* 107:12611–12616.
20. Kajiyama H, et al. (2008) Involvement of SDF-1alpha/CXCR4 axis in the enhanced peritoneal metastasis of epithelial ovarian carcinoma. *Int J Cancer* 122:91–99.
21. Okamoto T, et al. (2002) Clonal heterogeneity in differentiation potential of immortalized human mesenchymal stem cells. *Biochem Biophys Res Commun* 295: 354–361.
22. Yamashita Y, Tsurumi T, Mori N, Kiyono T (2006) Immortalization of Epstein-Barr virus-negative human B lymphocytes with minimal chromosomal instability. *Pathol Int* 56:659–667.
23. Shukla A, Stern M, Lounsbury KM, Flanders T, Mossman BT (2003) Asbestos-induced apoptosis is protein kinase C delta-dependent. *Am J Respir Cell Mol Biol* 29:198–205.
24. Al-Jamal KT, Kostarelos K (2010) Assessment of cellular uptake and cytotoxicity of carbon nanotubes using flow cytometry. *Methods Mol Biol* 625:123–134.
25. Stringer B, Imrich A, Kobzik L (1995) Flow cytometric assay of lung macrophage uptake of environmental particulates. *Cytometry* 20:23–32.
26. Jiang L, et al. (2008) Characteristics and modifying factors of asbestos-induced oxidative DNA damage. *Cancer Sci* 99:2142–2151.
27. Liu W, Ernst JD, Broaddus VC (2000) Phagocytosis of crocidolite asbestos induces oxidative stress, DNA damage, and apoptosis in mesothelial cells. *Am J Respir Cell Mol Biol* 23:371–378.
28. Tsuboi T, Fukuda M (2006) Rab3A and Rab27A cooperatively regulate the docking step of dense-core vesicle exocytosis in PC12 cells. *J Cell Sci* 119:2196–2203.
29. Tamura K, et al. (2009) Varp is a novel Rab32/38-binding protein that regulates Tyrp1 trafficking in melanocytes. *Mol Biol Cell* 20:2900–2908.
30. Vakarelski IU, Brown SC, Higashitani K, Moudgil BM (2007) Penetration of living cell membranes with fortified carbon nanotube tips. *Langmuir* 23:10893–10896.
31. Kostarelos K (2008) The long and short of carbon nanotube toxicity. *Nat Biotechnol* 26:774–776.
32. Fenoglio I, et al. (2008) Structural defects play a major role in the acute lung toxicity of multiwall carbon nanotubes: Physicochemical aspects. *Chem Res Toxicol* 21: 1690–1697.
33. Muller J, et al. (2008) Structural defects play a major role in the acute lung toxicity of multiwall carbon nanotubes: Toxicological aspects. *Chem Res Toxicol* 21:1698–1705.
34. Pulskamp K, Diabaté S, Krug HF (2007) Carbon nanotubes show no sign of acute toxicity but induce intracellular reactive oxygen species in dependence on contaminants. *Toxicol Lett* 168:58–74.
35. Toyokuni S (2009) Role of iron in carcinogenesis: Cancer as a ferrotoxic disease. *Cancer Sci* 100:9–16.
36. Guo L, et al. (2008) Adsorption of essential micronutrients by carbon nanotubes and the implications for nanotoxicity testing. *Small* 4:721–727.
37. Nagai H, et al. (2011) Asbestos surface provides a niche for oxidative modification. *Cancer Sci*, 10.1111/j.1349-7006.2011.02087.
38. Cheng JQ, et al. (1994) p16 alterations and deletion mapping of 9p21-p22 in malignant mesothelioma. *Cancer Res* 54:5547–5551.
39. Illei PB, Rusch VW, Zakowski MF, Ladanyi M (2003) Homozygous deletion of CDKN2A and codeletion of the methylthioadenosine phosphorylase gene in the majority of pleural mesotheliomas. *Clin Cancer Res* 9:2108–2113.
40. Altomare DA, et al. (2005) A mouse model recapitulating molecular features of human mesothelioma. *Cancer Res* 65:8090–8095.
41. Jean D, et al. (2011) Syntenic relationships between genomic profiles of fiber-induced murine and human malignant mesothelioma. *Am J Pathol* 178:881–894.
42. Kostarelos K, et al. (2007) Cellular uptake of functionalized carbon nanotubes is independent of functional group and cell type. *Nat Nanotechnol* 2:108–113.
43. Nimmagadda A, Thurston K, Nollert MU, McFetridge PS (2006) Chemical modification of SWNT alters in vitro cell-SWNT interactions. *J Biomed Mater Res A* 76:614–625.
44. Raffa V, et al. (2008) Can the properties of carbon nanotubes influence their internalization by living cells? *Carbon* 46:1600–1610.
45. Kostarelos K, Bianco A, Prato M (2009) Promises, facts and challenges for carbon nanotubes in imaging and therapeutics. *Nat Nanotechnol* 4:627–633.
46. Miserocchi G (1997) Physiology and pathophysiology of pleural fluid turnover. *Eur Respir J* 10:219–225.
47. Lacerda L, Raffa S, Prato M, Bianco A, Kostarelos K (2007) Cell-penetrating CNTs for delivery of therapeutics. *Nano Today* 2:38–43.
48. Muller J, et al. (2009) Absence of carcinogenic response to multiwall carbon nanotubes in a 2-year bioassay in the peritoneal cavity of the rat. *Toxicol Sci* 110: 442–448.
49. Toyokuni S (2009) Mechanisms of asbestos-induced carcinogenesis. *Nagoya J Med Sci* 71:1–10.
50. Chen GY, Nuñez G (2010) Sterile inflammation: sensing and reacting to damage. *Nat Rev Immunol* 10:826–837.
51. Hu Q, et al. (2010) Homozygous deletion of CDKN2A/2B is a hallmark of iron-induced high-grade rat mesothelioma. *Lab Invest* 90:360–373.
52. Okazaki Y, et al. (2010) A beverage containing fermented black soybean ameliorates ferric nitrilotriacetate-induced renal oxidative damage in rats. *J Clin Biochem Nutr* 47: 198–207.

Supporting Information

Nagai et al. 10.1073/pnas.1110013108

SI Materials and Methods

Characterization of Fibers. The lengths and widths of each fiber were determined by measuring at least 1,000 fibers with a high-resolution optical microscope (BZ-8000; Keyence) and a transmission electron microscope (JEM1400EX; JEOL). For the optical images, suspended fibers were spread over a glass slide, and a high-N.A. (1.40) lens was used. For transmission EM images, saline solution containing 0.5% BSA (A-saline solution)-suspended multiwalled carbon nanotubes (MWCNTs) and saline solution-suspended asbestos were spread directly over a copper grid with a plastic mesh and a carbon coat (cat. no. 653; Nisshin EM). After drying, fibers were analyzed. High-resolution transmission EM images were taken on a JEM-2100F (JEOL) high-resolution field-emission gun transmission electron microscope operated at 80 keV at room temperature under a pressure of 10^{-6} Pa. To determine the number of dispersed fibers in suspension, 0.5 mg/mL of the fiber suspensions was diluted to 0.05 mg/mL in saline containing 0.5% albumin. The diluted solution was then observed under a light microscope (BZ-8000). We counted the number of fibers inside a square with sides of 250 μm. In total, at least 16 fields of view were analyzed for each fiber type, and the concentration was calculated.

Establishment of a Mesothelial Cell Line. Human peritoneal mesothelial cells (HPMCs) were cultured from a resected omentum without peritoneal dissemination of an ovarian cancer patient as previously described (1). Written permission was obtained, and the procedure was approved by the Committee for Bioethics of the Nagoya University Graduate School of Medicine. The cells were grown in RPMI medium 1640 containing 10% FBS. The retroviral vectors, pCMSCVpuro-16E6E7 and pCMSCVneo-hTERT, were constructed by recombining segments of donor vectors (gifts from Tohru Kiyono, National Cancer Center, Tokyo, Japan) containing full-length HPV16E6 and E7 and the catalytic unit of human telomerase (2) using the Gateway system (Invitrogen) as previously described (3). Retroviral vectors encoding mCherry-human β-actin were produced by amplifying plasmid DNA from pmCherry-actin using PCR and the same set of primers. For attB1EGFPCherryCF, we used 5′-AAAAAGCAGGCTCCACCATGGTGAGCAAGGGCGA-3′ and attB2actinR 5′- AGAAAGCTGGGCTAGAAGCATTTGCGGTGGA-3′ and the adaptor primers 5′-GGGGACAAGTTTGTACAAAAAAGCAGGCT-3′ and 5′-GGGGACCACTTTGTACAAGAAAGCTGGGT-3′. After confirming the sequence, the Gateway system was used to generate pCMSCVneo mCherry-actin. HPMCs were infected at day 21 of culture with recombinant retroviruses containing E6 and E7 or mCherry-actin with the 10A1 envelope using 4 μg/mL Polybrene. Drug selection was then performed with 1 μg/mL puromycin or 0.2 mg/mL G418. For combinations of retroviral infections, E6 and E7-transduced cells were subsequently infected with the pCMSCVneo-hTERT-10A1 virus and then selected with G418.

Transmission EM to Evaluate Fiber Localization. We grew cells at 1×10^4 cells/cm^2 at 1 d before the addition of each fiber. Fibers were added at 5 μg/cm^2. The cells were fixed in phosphate buffer containing 2.5% glutaraldehyde and 2% paraformaldehyde after a 3-h incubation. The cells were then fixed with 1% osmium tetroxide and embedded in Epon resin, which was cut by a diamond knife into 80-nm or 500-nm ultrathin sections. The specimens were observed with a transmission electron microscope (JEM-1400EX; JEOL). Localization of fibers was determined by counting at least 30 randomly selected cells three times. In total, at least 100 cells were observed in each group.

Scanning EM to Evaluate Fiber Localization. We grew cells at 1×10^4 cells/cm^2 at 1 d before the addition of each fiber. Fibers were added at 5 μg/cm^2 and fixed in phosphate buffer containing 2% glutaraldehyde after a 3-h incubation. Cells were then rinsed, treated with 1% tannic acid and fixed again with 2% osmium tetroxide. Finally, cells were coated with osmium tetroxide at a thickness of 10 nm and observed with a scanning electron microscope (S-800S; Hitachi).

Cell Viability Assay Using Serum-Treated Fibers. Preparation of serum-treated fibers was performed by mixing equal amounts of FBS with the fiber suspension (0.5 mg/mL) at 37 °C for 30 min. The mixture was then centrifuged at 15,000 × *g* at 4 °C for 10 min, and the supernatants were discarded. The pellets were then suspended in culture medium.

Determination of Metal Concentrations. To measure the metals in the fiber suspensions, the supernatants were collected using the following procedure: centrifugation of the A-saline solution–suspended MWCNTs or saline-suspended asbestos (0.5 mg/mL) at 15,000 × *g* at 4 °C for 10 min, followed by careful collection of the supernatant and another centrifugation and collection step. For NT50a, NT50b, NT115, NT145, chrysotile (Chry), crocidolite (Cro), and amosite (Amo), we repeated the centrifugation and again collected the supernatant. For NTtngl, we performed ultracentrifugation at 300,000 × *g* at 4 °C for 30 min and collected the supernatant. The final supernatants were diluted 1:5 with deionized water. To measure the metals in the samples, 1 mL of each sample solution was completely reduced to ash by repeated treatment with nitric acid, hydrogen peroxide, and perchloric acid under heating at 200 °C. The sample ashes were dissolved in 9 mL of 7% nitric acid and then analyzed by inductively coupled plasma-MS by using an ICPM-8500 mass spectrometer (Shimadzu). We first measured magnesium, zinc, chromium, lead, nickel, and cadmium qualitatively and confirmed that the concentration of these metals in each sample was less than 10 ng/mL. Next, we measured the iron content (*m*/*z* 57) and the levels of copper (*m*/*z* 65). The concentration of both metals in each sample was calculated by using a standard curve for Fe and Cu (Wako). Values of a serially diluted standard solution displayed a linear regression with a straight line ranging from 10 to 100 ng/mL (ppb) for iron and from 1 to 100 ng/mL for copper. The measurement was performed at least five times (n = 5) to verify the results.

Electron Paramagnetic Resonance. We used an electron paramagnetic resonance spectrometer (JES-FR30; JEOL) to evaluate the free radical generation from each fibrous particle in the presence of hydrogen peroxide according to a previously described method (4) with slight modifications. The instrument settings were as follows: microwave frequency, 9.425 GHz; microwave power, 4 mW; modulation frequency, 100 kHz; modulation amplitude, 0.079 mT; sweep width, 5 mT; sweep time, 30 s; time constant, 0.1 s; center magnetic field, 336.2 mT and temperature, 290 K. We recorded the spectrum of the spin-trapped signals produced after 30 min of incubation at 37 °C. The reaction mixture was prepared by consecutively adding 20 μL of PBS solution (100 mM, pH 7.4), 60 μL of nitrilotriacetic acid disodium salt (5 mM), 80 μL of fiber suspension (5 mg/mL), 20 μL of 5,5-dimethyl-1-pyrroline-*N*-oxide (90 mM), and 20 μL

of hydrogen peroxide (100 mM). RDC-60-S disposable syringes (Radical Research) were used for the measurements.

Protein Adsorption on Fibers. We performed immunoprecipitation-like assay as previously described (5). FBS (100 μL) and each fiber (250 μg) were mixed, and RIPA (20 mM Tris-HCl, pH 7.4, 0.1% SDS, 1% Triton X-100, and 1% sodium deoxycholate) was added up to 1 mL In the case of HPMC lysate, 50 μg of cell lysate was mixed with each fiber suspension instead of serum. After a 3-h incubation at 37 °C, the mixture was centrifuged (15,000 X *g*) at 4 °C for 5 min. The supernatants were discarded, and the pellets were resuspended in RIPA buffer followed by two more cycles of centrifugation and resuspension. After the final centrifugation, we carefully discarded all supernatants, added SDS sample buffer, and boiled the samples for 10 min. The samples were centrifuged (15,000 × *g*) at 4 °C for 2 min, and the supernatants were evaluated by SDS/PAGE. The gel was silver-stained using a kit (Silver Staining Kit, Protein; GE Healthcare).

Fluorescent Images of Cellular Uptake of Fibers. MeT5A cells were cotransfected with actin-EGFP and either wild-type (WT) (6) or an inactive form (S34N) (7) of rab5a by using Lipofectamine 2000 (Invitrogen). The SSC value of EGFP-positive cells was then measured. The HPMCs were transfected with rab5a-GFP (Organelle Lights; Invitrogen) and actin-mCherry and observed under a fluorescent microscope (BZ-8000) at 5-min intervals after the addition of Cro, NT50a, and NT145. Representative images are shown in Fig. S1.

Raman Spectrometry. Raman spectra were measured in the back-scattering geometry by using a single monochromator and a microscope (HR-800; Horiba/Jobin Yvon) equipped with a CCD detector and a notch filter. The sample was excited by a He-Ne laser at 633 nm.

Quantitative RT-PCR Analysis. We grew RAW264.7 macrophages at a density of 5×10^4 cells/cm^2 at 1 d before the addition of each fiber. For each experiment, fibers were added to the culture medium to a final concentration of 0.1, 1 or 5 μg/cm^2. After 24 h, the total RNA was extracted with an RNeasy Plus Mini kit (Qiagen), and the cDNA was synthesized using the random primers, reverse transcriptase and buffer included in an RNA PCR kit (AMV; version 3.0; Takara). We used Platinum SYBR Green qPCR SuperMix-UDG (Invitrogen) and a 7300 real-time PCR system (Applied Biosystems) to conduct quantitative PCR. The expression of each mRNA (TNF-α, IL-1β, and IL-6) was normalized using 18S rRNA. The results show relative mRNA abundance compared with the control group. The primers used are as follows: 18S rRNA, sense (TCCTTTGGTCGCTCGCTCCT) and antisense (TGCTGCCTTCCTTGGATGTG); TNF-α, sense (GTGCCTATGTCTCAGCCTCT) and antisense (CTCCTCCACTTGGTGGTTTG); IL-1β, sense (CTCAACTGTGAAATGCCACC) and antisense (GAGTGATACTGCCTGCCTGA); IL-6, sense (CTTCTTGGGACTGATGCTGG) and antisense (CAGAATTGCCATTGCACAAC).

Immunohistochemical Analysis of Mesotheliomas. We prepared tissue arrays and performed immunohistochemistry as previously described (8, 9). Briefly, cores of 3 mm in diameter at representative areas were punched out, and six or 24 cores were embedded in a paraffin block that was sliced into 4-μm sections. We dewaxed sections that were attached onto slides in xylene and ethanol and subjected them to high-temperature antigen retrieval in an Immunosaver (Nisshin EM) for 40 min. After antigen retrieval, the slides were dipped in methanol containing H_2O_2 (0.3% vol/vol) to quench endogenous peroxidase activity for 30 min. After washing with PBS solution, slides were incubated with primary antibodies and washed with PBS solution three times for 5 min each. SimpleStain Rat multi (Nichirei) was applied to the slides followed by three washes with PBS solution. Localization of antigen-antibody complexes was visualized by liquid DAB+ (Dako) as brown precipitates before nuclear counterstaining with hematoxylin. Primary antibodies were as follows: anti–S-100 polyclonal antibody (LSL-LB-9197) was from Cosmo Bio, antidesmin monoclonal antibody (clone D33) was from Dako, antipodoplanin polyclonal antibody (KS-17) was from Sigma, anti-pan-cytokeratin monoclonal antibody (clone AE1/AE3) was from Thermo Fisher Scientific, and anti-mesothelin polyclonal antibody was from IBL (Immuno Biological Laboratories). Only in the case of desmin staining did we skip the antigen retrieval step.

Time-Lapse Microscopy. We grew MeT5A mesothelial cells or RAW 264.7 macrophages at 1×10^4 cells/cm^2 at 1 d before the addition of each fiber. Fibers were added at 5 μg/cm^2, and images were taken every minute for 3 to 4 h. The movies were made at a frame rate of 8 frames per second.

1. Kajiyama H, et al. (2008) Involvement of SDF-1alpha/CXCR4 axis in the enhanced peritoneal metastasis of epithelial ovarian carcinoma. *Int J Cancer* 122:91–99.
2. Okamoto T, et al. (2002) Clonal heterogeneity in differentiation potential of immortalized human mesenchymal stem cells. *Biochem Biophys Res Commun* 295: 354–361.
3. Yamashita Y, Tsurumi T, Mori N, Kiyono T (2006) Immortalization of Epstein-Barr virus-negative human B lymphocytes with minimal chromosomal instability. *Pathol Int* 56: 659–667.
4. Jiang L, et al. (2008) Characteristics and modifying factors of asbestos-induced oxidative DNA damage. *Cancer Sci* 99:2142–2151.
5. Nagai H, et al. (2011) Asbestos surface provides a niche for oxidative modification. *Cancer Sci*, 10.1111/j.1349-7006.2011.02087.
6. Tsuboi T, Fukuda M (2006) Rab3A and Rab27A cooperatively regulate the docking step of dense-core vesicle exocytosis in PC12 cells. *J Cell Sci* 119:2196–2203.
7. Tamura K, et al. (2009) Varp is a novel Rab32/38-binding protein that regulates Tyrp1 trafficking in melanocytes. *Mol Biol Cell* 20:2900–2908.
8. Hu Q, et al. (2010) Homozygous deletion of CDKN2A/2B is a hallmark of iron-induced high-grade rat mesothelioma. *Lab Invest* 90:360–373.
9. Okazaki Y, et al. (2010) A beverage containing fermented black soybean ameliorates ferric nitrilotriacetate-induced renal oxidative damage in rats. *J Clin Biochem Nutr* 47:198–207.

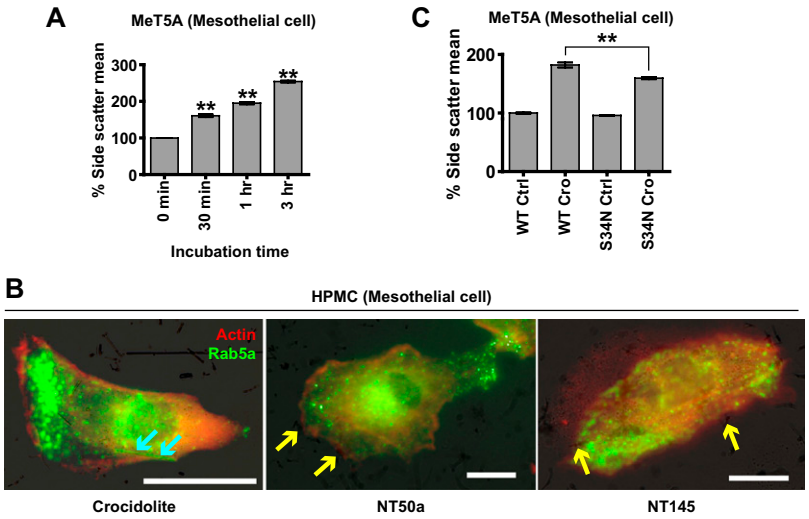

Fig. S1. Cro was internalized by mesothelial cells by an active signaling pathway that included rab5a. (*A*) Time-dependent increase in side scatter value of MeT5A cells after incubation with Cro. *P* values were calculated between 0 min (no addition of Cro) and the indicated times. (*B*) HPMCs transfected with rab5a-GFP and actin-mCherry internalized Cro with rab5a recruitment but did not internalize NT50a or NT145. Blue arrows indicate rab5a recruitment around the asbestos fiber whereas yellow arrows indicate lack of rab5a around nanotubes. (Scale bars: 20 μm.) (*C*) Mean of the side scatter value of each cell after a 3-h incubation with control (saline) or Cro. A partial inhibition of the increase in SSC value via cotransfection of the inactive form of rab5a (S34N) and actin-EGFP into MeT5A cells (**$P < 0.01$; $n = 3$, mean ± SEM). *P* values were determined by one-way ANOVA with post-hoc Tukey test.

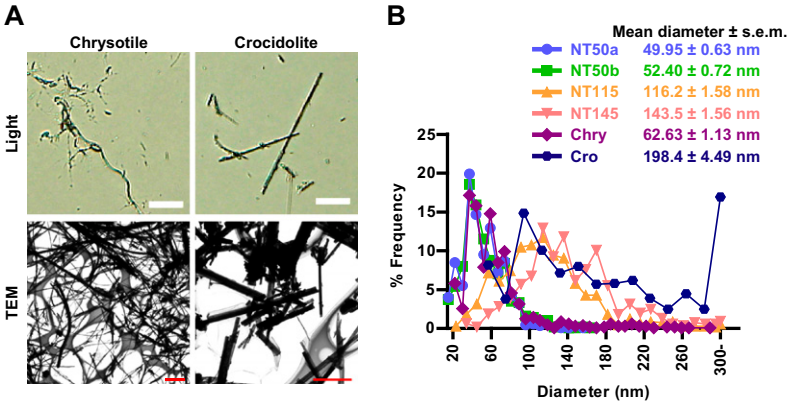

Fig. S2. Supplementary data for fiber diameter. (*A*) Optical images and transmission EM (TEM) images of Chry and Cro. (Scale bars: light microscopy images, 20 μm; transmission EM images, 2 μm.) (*B*) Distribution of the diameters of MWCNTs and asbestos.

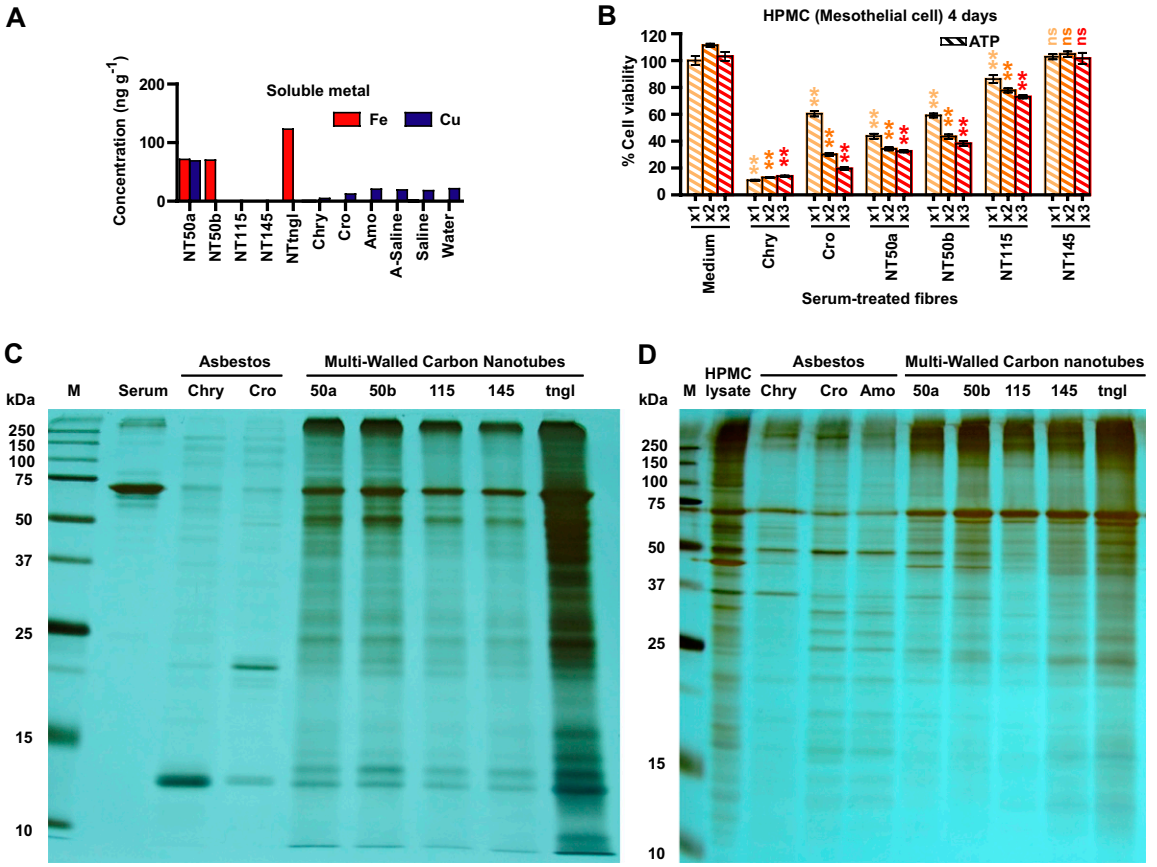

Fig. S3. Neither contaminating metals, serum depletion by fiber surface, nor protein adsorptive activity were the primary causes of mesothelial cell cytotoxicity by thin, dispersed MWCNTs with high crystallinity and rigidity. (*A*) Soluble metal (Fe and Cu) in each fiber solution (0.5 mg/mL). (*B*) ATP viability assay for HPMCs incubated with serum-treated fibers shows that NT50a (diameter ~ 50 nm) was severely cytotoxic, but NT145 (diameter ~ 150 nm) lacked cytotoxicity even at a density of 15 μg/cm^2 ($n = 4$, mean ± SEM; $^{**}P < 0.01$; ns, not significant). *P* values were determined by one-way ANOVA with post-hoc Tukey test. (*C* and *D*) Silver-stained gel after SDS/PAGE. Protein bands represent adsorptive proteins on the surface of the fibers (M, marker). Serum (*C*) and HPMC lysate (*D*) represent the original pattern. Each MWCNT type showed a similar profile in protein adsorption, but there was a difference in the amount of the adsorbed proteins. FBS (*C*) and HPMC lysate (*D*) were incubated with fibers as described in *SI Materials and Methods*.

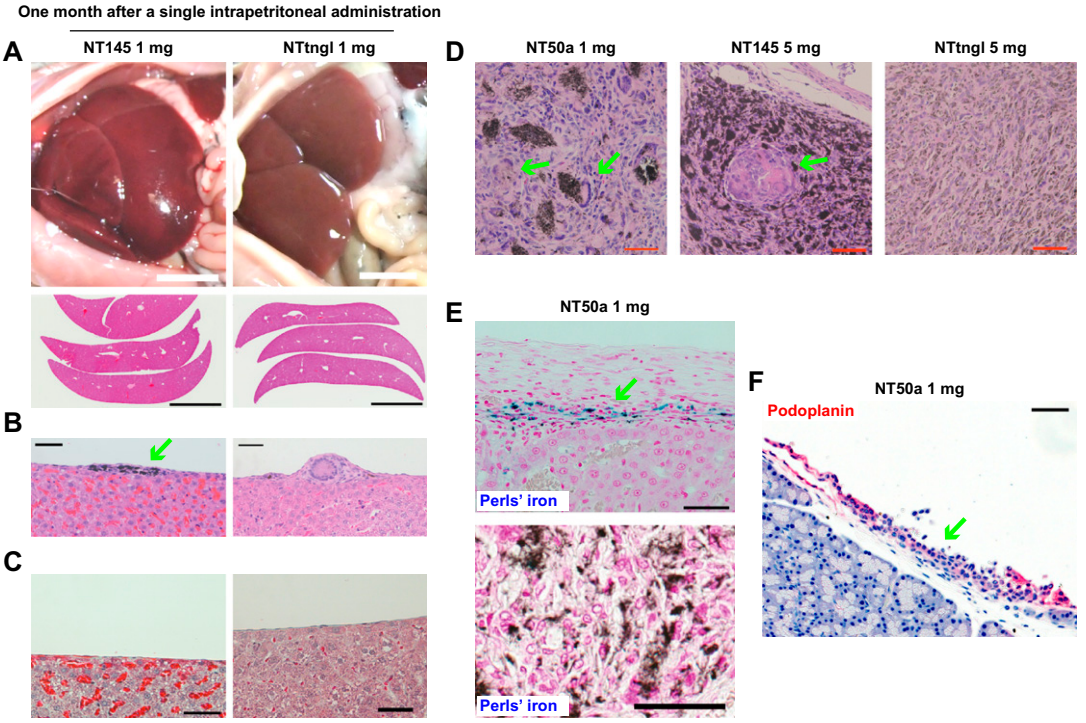

Fig. S4. NT50a uniquely induced iron deposition inside fibrotic tissue and mesothelial proliferation. (*A*–*C*) Macroscopic and microscopic images of rat organs 1 mo after a single i.p. injection of 1 mg NT145 (*Left*) or 1 mg NTtngl (*Right*). (*A*) Macroscopic images of i.p. organs just after dissection (*Top*). Low-power view of H&E-stained livers (*Bottom*). (Scale bars: 1 cm.) (*B*) Microscopic images of liver surface show the deposition of fibers (arrow) and little fibrotic responses around fibers. (*C*) Masson trichrome staining showing scarce light-green collagen. (*D*) Granuloma with multinuclear giant cells (arrow). (*E*) Perls' iron staining (blue) shows iron deposition (*Upper*, arrow) and shows that NT50a nanotubes are not stained (*Lower*) and thus that iron deposition (*Upper*) is a result of internal iron. (*F*) Immunohistochemistry for podoplanin (red) shows proliferation of mesothelial cells (arrow) in NT50a-injected rats. (Scale bars: *B*–*E*, 50 μm; *F*, 100 μm.)

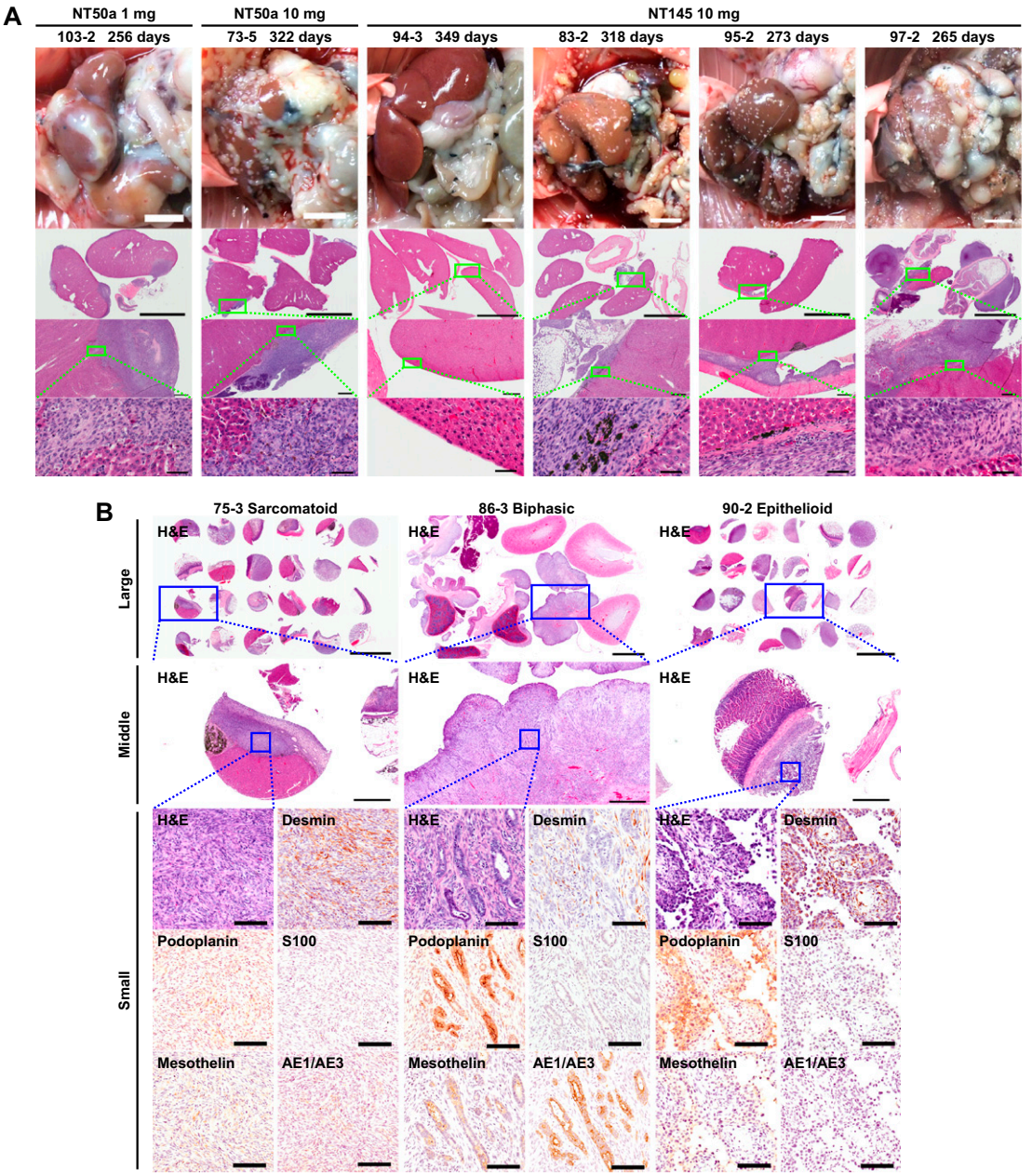

Fig. S5. Histopathology of mesothelioma. (*A*) Macroscopic images of i.p. organs just after dissection (*Top*). Low-power view of H&E-stained livers and other organs (*Bottom*). Microscopic images of mesothelioma invading liver parenchyma (103-2 and 73-5). Mesothelioma was not found in 94-3. Various extent of mesothelioma growth in rats injected with 10 mg NT145 (83-2, 95-2, and 97-2). (Scale bars: from top to bottom, 1 cm, 1 cm, 500 μm, and 50 μm.) (*B*) Immunohistochemistry of each specimen. (Scale bars: large, 5 mm; medium, 1 mm; small, 100 μm.)

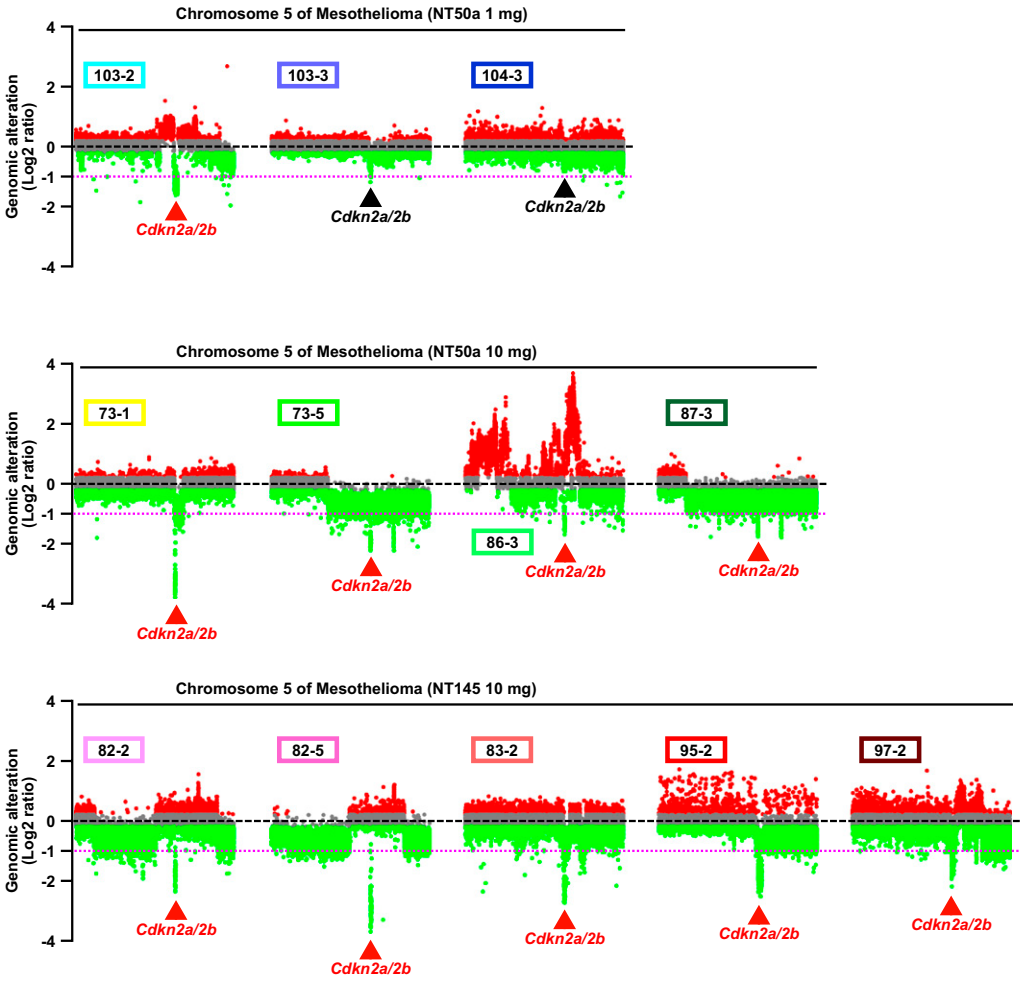

Fig. S6. *Cdkn2a/2b* was deleted in mesotheliomas induced by MWCNTs. Full scatter plot data for rat chromosome 5 indicates homozygous or heterozygous deletion of *Cdkn2a/2b*. Pink dotted lines decide whether the genomic deletion is homozygous ($y < -1$) or heterozygous. Red triangles indicate homozygous and black triangles indicate heterozygous or homozygous deletion. The numbers in squares indicate the identification number.

Table S1. Overall summary table of characteristics of MWCNTs

Characteristic*	NT50a	NT50b	NT115	NT145	NTtngl
Manufacturer	Mitsui	Showa Denko	Showa Denko	Showa Denko	Showa Denko
Diameter by the company, nm	50	80	150	150	15
Diameter by authors, nm	49.95 ± 0.63	52.4 ± 0.72	116.2 ± 1.6	143.5 ± 1.6	ND
Length by the company, μm	4	10	8	6	3
Length by authors, μm	5.29 ± 0.12	4.6 ± 0.10	4.88 ± 0.10	4.34 ± 0.08	ND
Aggregation extent	High	High	Low	Low	Very high
G/D ratio	6.7 ± 0.34	9.5 ± 1.0	7.0 ± 0.6	5.5 ± 0.6	1.5 ± 0.1
ROS generation via EPR (S/M)	0.27 ± 0.01	0.14 ± 0.03	0.20 ± 0.07	0.13 ± 0.03	0.24 ± 0.01
Phagocytosis by macrophages	Yes	Yes	Yes	Yes	None
Toxicity to macrophages	Moderate	Moderate	Moderate	Moderate	Very low
Piercing mesothelial cell membrane	Yes	ND	Low	Very low	None
Toxicity to mesothelial cells	High	High	Low	Low	Low
Inflammogenicity to rats	High	ND	ND	Low	Low
Carcinogenicity to rats	High	High	ND	Low	None

Values presented as mean ± SEM where applicable. EPR, electron paramagnetic resonance; G/D, graphite/defect; ND, not determined; ROS, reactive oxygen species; S/M, signal to marker ratio.
*0.5 mg/mL in A-saline solution.

Table S2. Mesotheliomagenesis experiment

	Female		Male		Total		Histology		
Name/dose, mg	Alive	Dead	Alive	Dead	Alive	Mesothelioma	Epithelioid	Biphasic	Sarcomatoid
NT50a									
-agg*	15	0	ND	ND	15	12	0	2	10
1	9	0	4	0	13	13	0	0	13
10[†]	23	12	20	5	43	43	1	7	34
NT50b									
10	6	5	ND	ND	6	6	0	1	5
NT145									
1	14	0	15	0	29	5	0	0	5
10	18	15	12	6	30	28	0	3	25
NTtngl									
10	9	4	6	6	15	0	0	0	0
A-saline (control)									
0	15	0	8	0	23	0	0	0	0

ND, not done; A-saline is vehicle control.
[†]Histological analysis was not possible in one case.

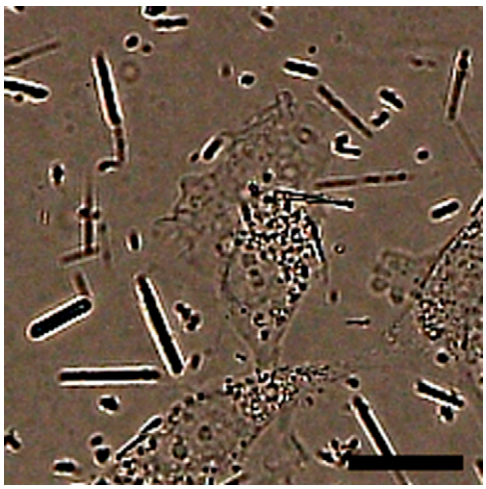

Movie S1. MeT5A mesothelial cells internalized Cro.

Movie S1

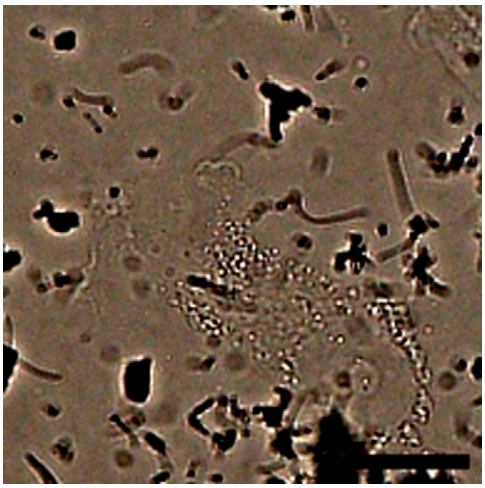

Movie S2. MeT5A mesothelial cells did not internalize NT115.

Movie S2

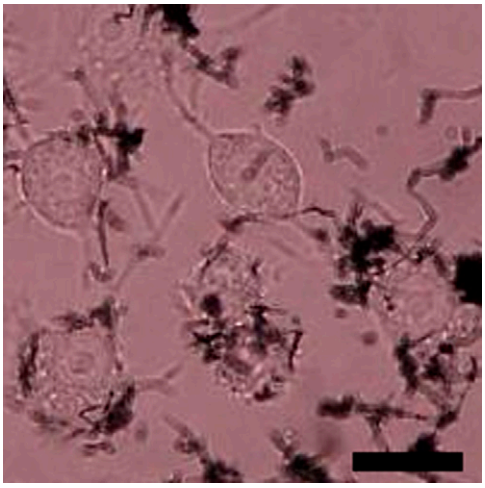

Movie S3. RAW264.7 macrophages phagocytosed NT145.

Movie S3

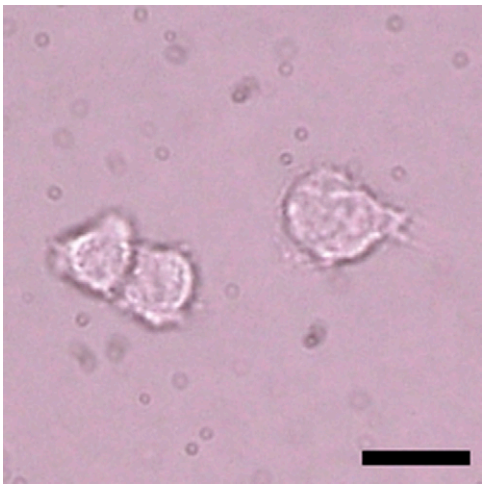

Movie S4. RAW264.7 macrophages did not phagocytose NTtngl.

Movie S4